General Disclaimer

One or more of the Following Statements may affect this Document

- This document has been reproduced from the best copy furnished by the organizational source. It is being released in the interest of making available as much information as possible.

- This document may contain data, which exceeds the sheet parameters. It was furnished in this condition by the organizational source and is the best copy available.

- This document may contain tone-on-tone or color graphs, charts and/or pictures, which have been reproduced in black and white.

- This document is paginated as submitted by the original source.

- Portions of this document are not fully legible due to the historical nature of some of the material. However, it is the best reproduction available from the original submission.

(NASA-CR-171284) FLOAT ZONE EXPERIMENTS IN SPACE Contractor Final Report, 1 Oct. 1983 - 30 Jun. 1984 (Ames Lab., Iowa.) 58 p
HC A04/MF A01 CSCL 22A

N85-15766

Unclas
G3/12 13418

NASA CONTRACTOR
REPORT

NASA CR-171284

FLOAT ZONE EXPERIMENTS IN SPACE

Ames Laboratory, USDOE
Iowa State University
Ames Iowa 50011

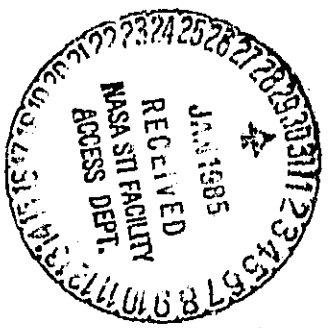

September 1984

Prepared for

NASA-George C. Marshall Space Flight Center
Marshall Space Flight Center, Alabama 35812

TECHNICAL REPORT STANDARD TITLE PAGE

1. REPORT NO.	2. GOVERNMENT ACCESSION NO.	3. RECIPIENT'S CATALOG NO.
NASA CR-171284		

4. TITLE AND SUBTITLE	5. REPORT DATE
Float Zone Experiments in Space	September 1984
	6. PERFORMING ORGANIZATION CODE JA64

7. AUTHOR(S)	8. PERFORMING ORGANIZATION REPORT #
J.D. Verhoeven, M.A. Noack, W.N. Gill, and C.C. Hsu	IS-4872, UC-25

9. PERFORMING ORGANIZATION NAME AND ADDRESS	10. WORK UNIT, NO.
Ames Laboratory, USDOE Iowa State University Ames, Iowa 50011	RTOP 179-80-70
	11. CONTRACT OR GRANT NO. H-34328B

12. SPONSORING AGENCY NAME AND ADDRESS	13. TYPE OF REPORT & PERIOD COVERED
National Aeronautics and Space Administration Washington, D.C. 20546	Contractor Report October 1, 1983 - June 30, 1984
	14. SPONSORING AGENCY CODE

15. SUPPLEMENTARY NOTES

Technical Manager: I. C. Yates, Marshall Space Flight Center, AL 35812
Final Report

16. ABSTRACT

The main goal of the float zone crystal growth project of NASA's Materials Processing in Space Program is to understand the molten zone/freezing crystal interface system and all the mechanisms that govern this system. If Marangoni convection produces oscillatory flows in the float zone of semiconductor materials, such as silicon, then it is unlikely that superior quality crystals can be grown in space using this process.

The major goals of this effort were: (1) to determine the conditions for the onset of Marangoni flows in molten tin, a model system for low Prandtl number molten semiconductor materials; (2) to determine whether the flows can be suppressed by a thin oxide layer; and (3) based on experimental and mathematical analysis, to predict whether oscillatory flows will occur in the float zone silicon geometry in space, and if so, could it be suppressed by thin oxide or nitride films.

Techniques were developed to analyze molten tin surfaces in a UHV system in a disk float zone geometry to minimize buoyancy flows. The critical Marangoni number for onset of oscillatory flows was determined to be greater than 4300 on atomically clean molten tin surfaces. Further work is necessary to attain the second and third goals. Analytical results indicate that the disk geometry is more stable than the cylindrical geometry and experiments may have to be conducted in space to attain the objectives.

17. KEY WORDS	18. DISTRIBUTION STATEMENT
Float zone; crystal growth; Marangoni flows; Materials Processing in Space	Unclassified - Unlimited James A. Downey III, Manager Spacelab Payload Project Office

19. SECURITY CLASSIF. (of this report)	20. SECURITY CLASSIF. (of this page)	21. NO. OF PAGES	22. PRICE
Unclassified	Unclassified	56	NTIS

Table of Contents

Summary - Overall Project

If Marangoni convection during float zone refining of semiconductor materials, such as Si, produces oscillatory flow, then it is nearly certain that space processing of such materials will not produce crystals of superior quality. The major goals of this project were (1) to determine the conditions for onset of oscillatory Marangoni flow in molten tin, a system which models the low Prandtl number molten semiconductors and then, (2) to determine whether the oscillatory flow, as well as steady Marangoni flow, could be suppressed by extremely thin tin oxide films, on the order of 6 to 100 A thick; and (3) based on the tin results and mathematical modelling analysis, to predict whether or not oscillatory flow will occur in the float zone silicon geometry, and if so could it be suppressable by means of films such as oxides or nitrides at the nanometer level of thickness.

The project involved: (1) Developing an experimental technique for float zone solidification which minimized bouyancy driven convection, and allowed in situ Auger analysis of the molten Sn surface. (2) Developing surface analytical techniques to measure tin oxide films down to monolayer thicknesses. (3) Mathematical modelling to guide the experimental research and ultimately address goal 3.

The project was funded for 5.75 years at a level adequate to support one full time experimental scientist (Max Noack), 10 to 15% of the P.I. (J. D. Verhoeven) and half support for a graduate student (C. C. Hsu) and around 10 to 15% of a consulting staff member. During the second and third year Dr. A. J. Bevolo consulted on problems concerning

Auger analysis. During the third year, work began with Dr. W. N. Gill and graduate student C. C. Hsu on mathematical modelling, and Dr. Gill was supported as a consultant during the final 1.75 years of the project, and Hsu was supported half time for two years.

Following are a list of the accomplishments of the project.

1) Techniques were developed to analyze molten tin surfaces in a UHV system.[1,2,3] It was discovered that the Auger CMA could be used to do ELS (electron loss spectroscopy) and that by so doing the minimum thickness at which the oxide film could be detected to be continuous was extended to considerably lower values than with Auger analysis alone.

2) A disk float zone (DFZ) geometry was developed[1,4] which allowed bouyancy flows to be minimized (Bond number ≈ 0.05) and allowed Auger/ELS analysis on flat molten surfaces. The technique was extended to a model system, $NaNO_3$, and Marangoni flow was demonstrated.[5]

3) Experiments were carried out in a UHV environment which showed that with the disk geometry, $(Ma)_{CR}$ for onset of oscillatory flow is greater than 4300 on atomically clean molten Sn surfaces (unless the frequency of oscillation is greater than around 10 Hz).[8]

4) Both a finite difference analysis and an approximate boundary layer analysis have been carried out for the DFZ geometry.[6-9] The finite difference analysis shows that for conditions of the Ma ≈ 4300 experiment, surface velocities of 25 cm/s are expected; quite good agreement was found between the boundary layer analysis and the finite difference analysis.

5) The boundary layer analysis was extended to other geometries[8,9] and it was found that for cylindrical geometries multiple solutions occur at critical values of the parameter $2(d/\ell)^3$ (Ma/Pr), which suggests flow instabilities; whereas for the disk geometry, no multiple solutions were found. This result suggests that the disk geometry may be considerably more stable to oscillatory flow than the cylindrical geometry characteristic of float zone configurations.

Publications Resulting from this Project

1. J. D. Verhoeven, M. A. Noack and A. J. Bevolo, Suppression of Marangoni Convection with Oxide Films, Processing in the Reduced Gravity Environment of Space, Materials Research Society Symp. Proceedings, Vol. 9, 513-522, Ed. by Guy Rindone, North Holland, N.Y. (1982).
2. A. J. Bevolo, J. D. Verhoeven, and M. Noack, Electron Loss Study of Native Oxide of Tin, J. Vac. Sci. Tech. 20(4), 943 (1982).
3. A. J. Bevolo, J. D. Verhoeven and M. Noack, A Low Energy Electron Loss and Auger Study of the Oxidation of Liquid and Solid Tin, Surface Science 134, 499 (1983).
4. W. N. Gill, C. C. Hsu, J. D. Verhoeven and M. Noack, Thermocapillary and Buoyance Driven Flows in Liquid Metal Disks. Proceedings of PACHEC '83, Vol. I, I38-44 (1983).
5. C. C. Hsu, W. N. Gill, M. A. Noack and J. D. Verhoeven, Marangoni Flow Velocity in a Thin Disk of Molten $NaNO_3$, Chem. Engr. Comm. 24, 167-376 (1983).
6. W. N. Gill, Floating Zone Crystallization, Symposium on Separation Technology, 206-210, Taipai (1983).

7. W. N. Gill, Surface Tension Driven Boundary Layer Flow in Floating Zones, Chem. Engr. Comm. 23, 57 (1983).

8. W. N. Gill, N. D. Kazarinoff, C. C. Hsu, M. A. Noack and J. D. Verhoeven, Thermocapillary Driven Convection in Supported and Floating Zone Crystallization, COSPAR, Advances in Space Research, Pergamon Press, (1984 or 85).

9. W. N. Gill, N. D. Kazarinoff and J. D. Verhoeven, Convective Diffusion in Zone Refining of low Prandtl Number Liquid Metals and Semi-conductors, Symposium on Chemical and Physical Processing of Integrated Circuits, ACS Symposium Series (1984 or 85).

Summary - Incompleted Work

Unfortunately, the project never accomplished its major goals of establishing $(Ma)_{CR}$ values for onset of oscillatory flow in molten Sn and of determining the effectiveness of tin oxide on suppressing both oscillatory and steady Marangoni flow. It is felt that with an additional year or two of funding the experiments could have been extended to Ma values greater than 10,000, where Schwabe has observed oscillatory flow in cylinder geometries of a Pr = 9 fluid. Also, the effect of oxides on macrosegregation, and therefore on Ma flow, could have been evaluated, using radioisotope techniques; and further theoretical work could have been performed on the influence of adsorbed oxygen and oxides on Marangoni flows in liquid metals and semiconductors.

The contract terminated before a stability analysis could be performed on the nonlinear multiple solutions which were obtained for the base flows. It has been shown clearly in the paper listed as Reference 9 above (attached in full, starting on page 18) that the pressure distribution in the zone is intimately related to both nonlinear inertial effects in Marangoni flows and to the surface deflection, and this is conjectured to be important in hydrodynamic and thermal stability. The analysis of surface deflection for a supported cavity or slot, which appears in this paper, applies in large measure to the disk geometry also. It shows for the first time that the surface deflection, the pressure distribution, the parameter $Re\ A/\varepsilon$, and the parameter A^3Re (which reflects the importance of nonlinear flow effects) are intimately related. It is conjectured that this interaction has an

important influence on flow stability in the zone and may explain why existing stability analyses predict critical parameter values an order of magnitude too low.

Summary of Work done October 1, 1983 to June 30, 1984

We were informed at the beginning of this year, October 1983, that the project would be terminated after nine months, in June 1984. With this limitation in mind, and given the goals of the project which are listed on page 1, we decided to concentrate the experimental work in the following three areas:

1) Attempt to determine the onset of oscillatory Marangoni flow in the DFZ apparatus, using miniature thermocouples to detect oscillatory flow.

2) Attempt to detect changes in solid-liquid interface shapes in the DFZ samples due to presence of Marangoni flow.

3) Attempt to determine the effect of Marangoni flow upon macro-segregation during plain front solidification experiments in the DFZ samples.

In summary, the work progressed as follows: The experiments in the second area were unsuccessful because of an unanticipated effect which is described in the following report. The experimental work in the first area was successful, but showed that we were limited to a maximum Ma number of 4300 with our present heater, at which value no detectable oscillations occurred. Because development of a new heater would take too long a decision was then required on whether to push the present heater beyond design limitations and risk burnout, or to start the third area of experimental work. The decision was made to start on the third experiment and it was only partially completed by project termination on June 30.

The major results of the final nine months work involve experimental results from the first area and theoretical modelling work, both of which are presented in our July 1984 COSPAR paper. In addition, the theoretical modelling work (including some work done on non NASA funding since the June termination) has been prepared for an ACS review paper. Hence, the report which follows includes essentially 3 sections:

I. Paper presented at the July 1984 COSPAR Conference in Graz, Austria and to be published by Pergamon Press (1984 or 85).

THERMOCAPILLARY DRIVEN CONVECTION IN SUPPORTED AND FLOATING ZONE CRYSTALLIZATION

W.N. Gill,* N.D. Kazarinoff,** C.C. Hsu,*** M.A. Noack,† and J.D. Verhoeven†

*Chemical Engineering Department, **Mathematics Department, State University of New York at Buffalo, Amherst, NY 14260, U.S.A.
***Chemical Engineering Department, †Metallurgy Department, Iowa State University, Ames, IA 50011, U.S.A.

ABSTRACT

Marangoni flow was induced in a thin disk of molten tin with an atomically clean surface by heating it from below in an ultra high vacuum apparatus. The radial distribution of temperature was measured and no temperature oscillations were observed. Strong mechanical disturbances introduced at a Marangoni number of about 4300 died out quickly with time indicating that the system was stable. Mathematical models indicate that strong flows in a two cell structure exist under the conditions studied, and that the velocity profile in the cell near the surface is of the boundary layer type which varies rapidly with depth.

INTRODUCTION

The importance of the development of high quality single crystalline silicon in the evolution of the current "high-tech" solid state industry is clear. A significant limitation to the quality of single crystal silicon is the presence of growth striations, which result from oscillatory convective flows present in the molten Si at the solid-liquid interface during growth of the Si crystals from the melt. Because of natural convection, it is extremely difficult to eliminate these oscillatory flows at 1-g, but in space one expects no oscillatory flows from the buoyancy force. Hence, the preparation of Si single crystals free of striation defects is a potential application for space processing. Although it is not at all clear that practical economics would favor such an operation, it is very difficult to predict these economics now for the long range future with the advent of such technologies as a space station. Therefore, it seems important that the potential of space processing for the preparation of striation free semiconductor materials be established.

Several experiments /1,2,3/ have shown that oscillatory Marangoni convection occurs in high Prandtl number liquids. At present there is little agreement concerning the proper dimensionless parameter to be used to characterize the critical physical conditions for the onset of such oscillatory flow, and there are no experiments known to us which have demonstrated oscillatory Marangoni convection in low Prandtl number liquids such as molten metals and semiconductors. If Marangoni convection during float zone refining of semiconductor materials such as Si produces an oscillatory flow, then it is nearly certain that space processing of such materials will not produce the hoped for striation free crystals of superior quality. Hence, the question of the conditions required for the onset of Marangoni flow in low Prandtl number liquids has important practical implications, as well as interesting theoretical implications. This paper presents results of some initial experimental and theoretical studies on this problem.

The zone studied both experimentally and theoretically is a circular disk of pure tin heated from below by a tantalum heater and cooled around the periphery of the disk by an oil bath whose temperature was controlled. The disks, which were approximately 1 to 1.2 mm in height and 15 mm in radius, rested on the tantalum heater which varied from 1.75 to 3 mm in radius. By varying the power to the heater and controlling the temperature of the oil bath, molten zones of tin with radii from about 4 to 6.5 mm were produced.

Differences between the high temperature at the center of the disk and the solid-liquid interface at the periphery of the molten zone ranged from about 50 to 140°C, and average temperature gradients across the disk varied from approximately 115 to 250°C/cm.

Mathematical Model and Analysis of Surface Tension Driven Flow in Liquid Metal Disks

Two approaches have been taken here to model the surface tension driven flow in a liquid metal disk. In the first we have used a finite difference analysis of the Navier-Stokes and

energy equations and boundary conditions which closely represent the real physical system under consideration. In the second, more simplified approach, we have neglected "end effects" and have assumed that the liquid region is unbounded in the radial direction which enables one to reduce the Navier-Stokes equations to an ordinary differential equation. These approaches are complementary in that both of them retain the essential nonlinear features of the problem, and the simplified approach suggests ways that the more detailed finite difference calculations can be correlated and interpreted. The simplified model also enables one to search for multiple steady state solutions of the problem and thereby get some indication of the effect of the physical and geometrical parameters on the hydrodynamic stability of the Marangoni flows, which occur in the materials and configurations of interest in crystal growth.

The equations of motion and energy for a disk heated uniformly from below with a flux q over the radius a, and symmetrically with respect to its axis are

$$\frac{\partial ru}{\partial x} + \frac{\partial rv}{\partial r} = 0 \tag{1}$$

$$u\frac{\partial u}{\partial x} + v\frac{\partial u}{\partial r} = -\frac{1}{\rho}\frac{\partial P}{\partial x} + \nu\left|\frac{\partial^2 u}{\partial x^2} + \frac{1}{r}\frac{\partial}{\partial r}\,r\,\frac{\partial u}{\partial r}\right| + \frac{\rho}{\rho_m}\,g_x \tag{2}$$

$$u\frac{\partial v}{\partial x} + v\frac{\partial v}{\partial r} = -\frac{1}{\rho}\frac{\partial P}{\partial r} + \nu\left|\frac{\partial^2 v}{\partial x^2} + \frac{\partial}{\partial r}\frac{1}{r}\frac{\partial}{\partial r}\,rv\right| + \frac{\rho}{\rho_m}\,g_r \tag{3}$$

$$u\frac{\partial T}{\partial x} + v\frac{\partial T}{\partial r} = \alpha\left|\frac{\partial^2 T}{\partial x^2} + \frac{1}{r}\frac{\partial}{\partial r}\,r\,\frac{\partial T}{\partial r}\right| \tag{4}$$

The coordinate r is measured from the axis of the disk and x is measured from the upper surface down into the fluid, the total depth of fluid being d.

The boundary conditions are

$$v(x,0) = u(d,r) = v(d,r) = 0, \quad 0 \le r \le a \tag{5}$$

$$u(x,\ell) = v(x,\ell) = 0 \tag{6}$$

$$\mu\frac{\partial v}{\partial x}(0,r) = \left|\frac{d\sigma}{dT}\right|\frac{\partial T}{\partial r}(0,r) \tag{7}$$

$$\mu\frac{\partial v}{\partial x}(d,r) = \left|\frac{d\sigma}{dT}\right|\frac{\partial T}{\partial r}(d,r), \quad a \le r \le \ell \tag{8}$$

$$k\frac{\partial T}{\partial x}(d,r) = q, \quad 0 \le r \le a \tag{9}$$

$$k\frac{\partial T}{\partial x}(d,r) = 0, \quad a \le r \le \ell \tag{10}$$

$$k\frac{\partial T}{\partial x}(0,r) = k\frac{\partial T}{\partial r}(x,0) = 0 \tag{11}$$

$$T(x,\ell) = T_m \tag{12}$$

where ℓ is the radius of the molten zone and T_m is the melting point.

Finite difference solutions to equations (1-12) were obtained for Prandtl number, $Pr = \nu/\alpha$, equal 0.014, the Pr of tin, and for $Pr = 0.02$, 9, the latter being the Pr of $NaNO_3$. To check the accuracy of the calculations by being able to compare them with experimental data some solutions with $Pr = 9$ were obtained for a cavity and these results compare very favorably with the surface velocities measured by Schwabe and Scharmann /1/ for $NaNO_3$. The agreement between our calculations and the experiments is especially good above a ΔT of 35°C in which case the entire cavity was liquid.

Figure (1) shows a comparison between the temperature distributions predicted by assuming only diffusion in the melt (no convection), and a constant heat flux over $0 \le r \le \ell$, and those obtained from the finite difference analysis of equations (1-4), which includes both conduction and convection. One sees that the pure conduction solutions differ rather little from the temperature distribution produced by Marangoni convection until the value of Ma exceeds 2500. Thus, because of the high thermal conductivity of liquid metals, one can obtain a reasonably good representation of the temperature distribution by neglecting convection completely unless Ma is large. This suggests that considerable information about Marangoni flow may be obtained by using a simplified surface temperature distribution in solving the equations of motion if one is interested primarily in low Prandtl number fluids such as liquid metals or semi-conductors.

If view of the preceding discussion, we decided to simplify markedly the problem as follows: In addition to assuming that the free surfaces are flat, we assumed that surface heating is

accomplished with a heat flux which will produce a parabolic temperature distribution on the surface of the disk. Therefore the temperature distribution on the disk surface is given by

$$T_S = T_{HOT} - \left(T_{HOT} - T_{COLD}\right)\left(\frac{r}{\ell}\right)^2 \tag{13}$$

One can show that as $Pr \to 0$, a constant heat flux on the surface will produce precisely the distribution given by equation (13). In equation (13), T_{HOT} corresponds to the temperature at $r = 0$ and T_{COLD} represents that at $r = \ell$. That is, ℓ is simply the distance over which one measures the temperature difference ΔT. Equation (13) is the pure conduction solution plotted in Figure 1.

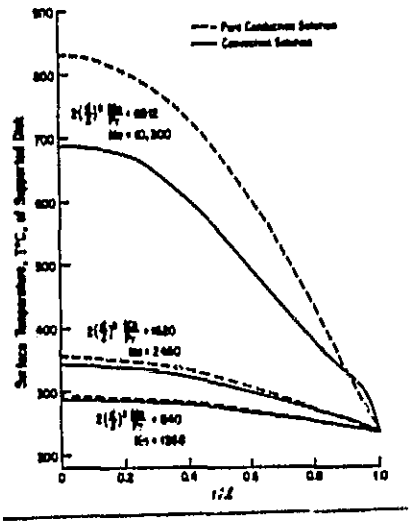

Fig. 1. Comparison of pure conduction with $a/\ell = 1$ and convection with $a/\ell = 0.875$ solutions for disks with $\ell/d = 6$ and various Marangoni numbers.

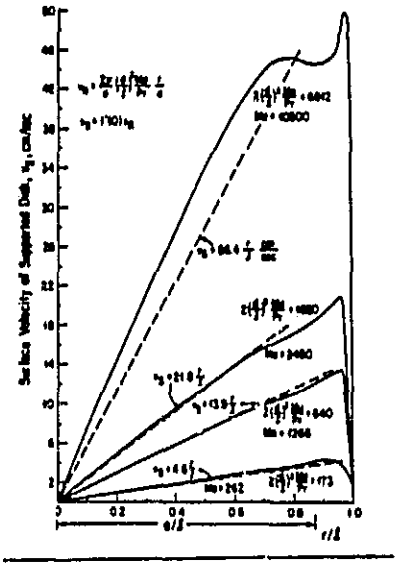

Fig. 2. Surface velocity distribution for disk with $\ell/d = 6$. Comparison of simplified model with finite difference solution for various Ma.

We further assume that "no end effects" exist. This means that the flow is not obstructed by a solid surface at $r = \ell$. With these assumptions, one can obtain exact solutions of equations (1-3, 5-7) as follows. Define a stream function ψ as usual by

$$rv = \frac{\partial \psi}{\partial x}, \quad -ru = \frac{\partial \psi}{\partial r} \tag{14}$$

and let ψ take the form

$$\psi = rd\, v_R \int_0^\eta \frac{v}{v_R}\, d\eta = rd\, v_R f(\eta) \tag{15}$$

where $\eta = x/d$ and v_R is a function of r only. One can show readily that $v = v_R f'$ and $u = -fd\, dv_R/dr$ and thus equations (1-3) are reduced to

$$f''' + 2\left(\frac{d}{\ell}\right)^3 \frac{Ma}{Pr}\left|2ff'' - f'^2\right| = \frac{d^2}{\mu v_R}\frac{\partial P}{\partial r} = \beta \tag{16}$$

with

$$f(0) = f(1) = f'(1) = f''(0) + 1 = 0 \tag{17}$$

for a supported disk and

$$f(0) = f(1) = f''(1) = f''(0) + 1 = 0 \tag{18}$$

for a floating disk if the velocity scale, v_R, is

$$v_R = \frac{2\nu}{d}\left(\frac{d}{\ell}\right)^2 \frac{Ma}{Pr}\frac{r}{\ell} \tag{19}$$

and if d is interpreted as the thickness (or height) of the supported disk and the half-thickness of the unsupported disk, and ν is the kinematic viscosity. The coordinate x is measured from the free surface into the fluid, and $g_x = g_r = 0$.

The quantities on the lefthand side of equation (16) are functions of η only, and those on

the right are only of r. Therefore β is a constant which can be determined with the aid of the boundary conditions given in equations (17) and (18). Note that solutions of equations (16) to (18) depend only on the single parameter $2(d/\ell)^3 Ma/Pr$ and computations were carried out for supported and floating disks up to values of the parameter equal to 90,000.

Figure 2 shows some comparisons between the finite difference calculations of surface velocities and those predicted for the supported disk by equation (16) with the boundary conditions (17). It is seen that the agreement is excellent over 80% of the disk and in this case, for the finite difference computations, the disk was heated uniformly only over 87.5% of its radius as indicated by the value of a/ℓ at the bottom of Figure 2. Thus, the end effects are due to both the solid-liquid interface and the fact that the heater does not cover the entire liquid region as is assumed in the simplified model. Also, it is clear that the agreement is better at lower values of Ma, where conduction predominates and the simplified model results are essentially indistinguishable from the finite difference solution. Note that the finite difference solutions show a double peak structure at larger values of Ma, as shown by the solid lines in Figure 2.

The surface velocity distribution obtained from this simplified model is given by Figure 3 in which v_R is given by equation (19). Clearly, $v_S/v_R = f'(0)$, is a function only of $(d/\ell)^3 Ma/Pr$ as is the local velocity field when v_R is used as the velocity scale. It is noteworthy that the v_S/v_R ratio for both floating and supported disks is essentially the same except at small values of $2(d/\ell)^3 Ma/Pr$, when d is interpreted as indicated.

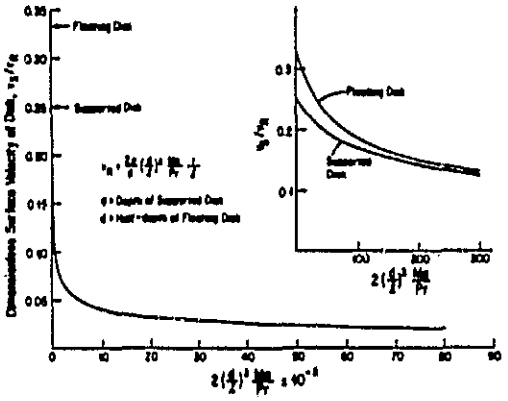

Fig. 3. Dimensionless surface, velocity, v_S/v_R as a function of $2(d/\ell)^3 Ma/Pr$ for supported and floating disks.

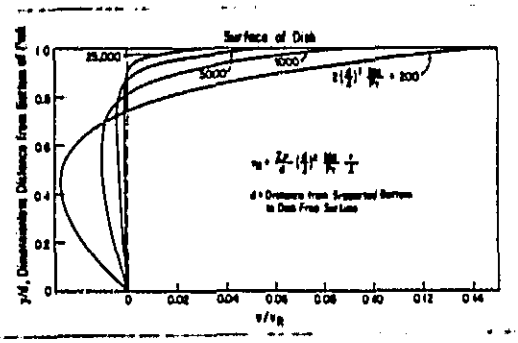

Fig. 4. Dimensionless steady state radial velocity profiles for surface tension driven flow in disk supported on bottom.

Radial velocity profiles as functions of distance from the surface of the disk are shown for the simplified model in Figures 4 and 5 for supported and floating disks, respectively. The value of the parameter $2(d/\ell)^3 Ma/Pr$ is varied by two orders of magnitude to demonstrate how the shape of the velocity field changes with changes in either geometry, d/ℓ, or heat flux, Ma. One sees that the depth, over which the velocity changes from the value at the surface to zero decreases from about 28% - 30% of the disk height to about 7% - 10% as the characteristic parameter increases from 200 to 25,000. Furthermore, the velocity in most of the core of the floating disk is almost constant at higher heating rates and as the depth to radius of the molten zone increases.

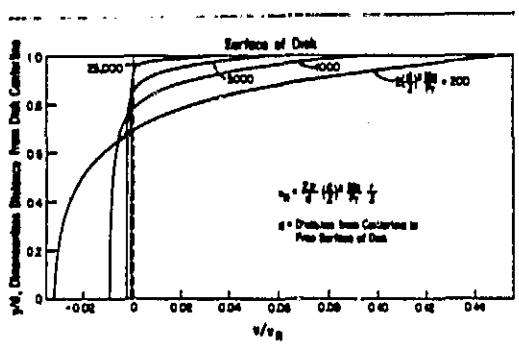

Fig. 5. Dimensionless steady state radial velocity profiles for surface tension driven flow in floating disk.

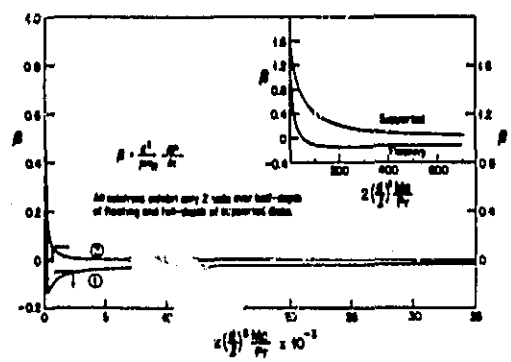

Fig. 6. Steady state solutions of Navier-Stokes equations for surface tension driven flow in floating (1) and supported (2) disks.

Figure 6 illustrates how the dimensionless pressure gradient parameter, B, (which is a constant for a given value of $2(d/\ell)^3 Ma/Pr$) varies with the characteristic parameter, $2(d/\ell)^3 Ma/Pr$. One sees that B varies very slowly beyond values of 5000 for the characteristic parameter and at values of 90,000 B equals 1.1×10^{-8} for the supported disk and -1.22×10^{-2} for the floating disk. Over the range of 0 to 90,000, no evidence of multiple steady state solutions to equations (16-18) was found for either the supported or floating disks. The radial velocity profiles all exhibit only two cells, one radially outward and one radially inward, for all values of $2(d/\ell)^3 Ma/Pr$. This rather stable behavior is in dramatic contrast to that which we have found for the cavity and the cylinder, both of which evidence multiple steady-state solutions and are less stable configurations from a fluid mechanical viewpoint.

Experimental Results

Molten tin was chosen for study because its low Prandtl number, 0.014, and its tendency to oxidize are typical of molten metals and semiconductors; and because its low vapor pressure makes it amenable for study in a vacuum. It is generally agreed that the strong tendency of molten metals and semiconductors to form oxide films on their surfaces will have a pronounced effect on Marangoni convection. Therefore an experimental design was developed which employed ultra high vacuum (UHV) techniques incorporating both an argon ion sputter gun to clean the molten tin surface and an Auger analyser to examine the molten tin surface *in situ* and verify that it is free from oxides. The system utilizes a disk float zone (DFZ) geometry which is shown schematically in Fig. 7. A tin disk of diameter 2R and height d is cooled around its periphery by a copper cylinder whose temperature is controlled by flowing hot oil supplied from an external constant temperature bath. The tantalum heater at the bottom center of the disk produces a molten zone of diameter 2ℓ in the disk. The entire system is within a UHV chamber capable of achieving a vacuum of 2×10^{-10} Torr with the system at temperature.

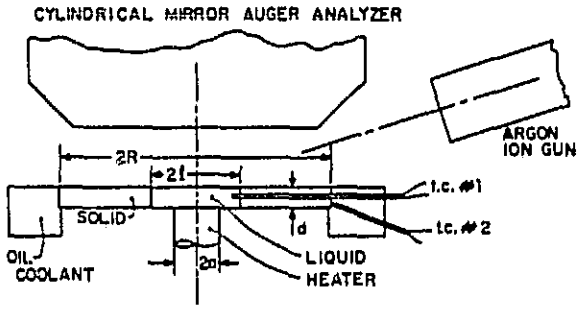

Fig. 7. Schematic representation of the disk float zone configuration.

Two types of experiments were performed on the tin disks. In the first type, temperature traverses were made using a miniature thermocouple, which in some cases was W-Re with 50 μm wires, the bead of which was inserted directly in the molten metal and in other cases involved a 25 mm OD thermocouple which was chromel-alumel (type K) and was contained within a stainless steel tube plated with pure chromium, which was slightly oxidized to avoid reaction with the molten tin.

Accurate experimental temperature distributions were obtained from these traverses, and two typical ones are shown in Figure 8. In Figure 8, we also include temperature distributions calculated from solutions for the profile of temperature averaged over the height of the disk, $\overline{T}$, which are given by

$$\overline{T} = T_{melt} - \frac{qa^2}{4k_L d}\left(\frac{r^2}{a^2}\right) + \frac{qa^2}{4k_L d}\left|1 + 2\,\ell n\,\frac{\ell}{a}\right| \tag{20}$$

for the region inside the heater, and

$$\overline{T} = T_{melt} - \frac{qa^2}{4k_L d}\,\ell n\,\frac{r}{\ell} \tag{21}$$

for the region outside the heater which supplies power, $P = \pi a^2 q$, given by

$$P = 2\pi\, k_S d\,\frac{\left(T_{sink} - T_{melt}\right)}{\ell n\ R/\ell} \tag{22}$$

Equations (20) and (21) assume no radiation loss from the tin to the vacuum surrounding it because this can be shown to be small.

One sees in Figure 8 that the temperature distribution given by equations (20) - (22), in which the thermal conductivity of the liquid phase, k_L, is 0.32, j/cm°C, is consistently higher than the experimental results. Note that the heat flow is predominantly radial in the disk, and we interpret the differences obtained in the experiments between the centerline temperatures and the melting point being smaller than those calculated by equations (20 - 22) to be strong evidence that Marangoni flow exists in the liquid melts studied. However, the temperatures measured were very stable as predicted by the simplified models, and there is no evidence of oscillatory flow. Because very thin disks were used, the maximum Bond numbers for our experiments was about 0.05. Therefore, natural convection was negligibly small as confirmed by a finite difference simulation of run 58. The second type of experiment was conducted to determine if we could induce thermal oscillations in the system by perturbing it strongly after we had created the largest temperature difference, disk size and Marangoni number that we could on earth without having the molten zone fall out. This experiment was run as follows. After achieving UHV conditions, the oil sink temperature was adjusted to 166°C as measured by t.c. #2, and a molten zone with a diameter around 8 mm was achieved. The Argon ion sputter gun then was turned on and the molten surface was cleaned by moving the beam over it. Both Auger and Low Energy Electron Loss (LEEL) signals were used to be sure that the surface was free of oxide. The thermocouple within the molten zone was monitored on a strip chart recorder to detect possible oscillations resulting from oscillatory Marangoni flow. This procedure was repeated with increased power and the maximum molten tin diameter achieved in this experiment was 11.7 mm. The thermocouple tip was positioned at a radius of 3 mm.

Temperature oscillations were not detected in this experiment which indicates that oscillatory Marangoni flow probably was absent. There are four important questions regarding this conclusion which will now be addressed.

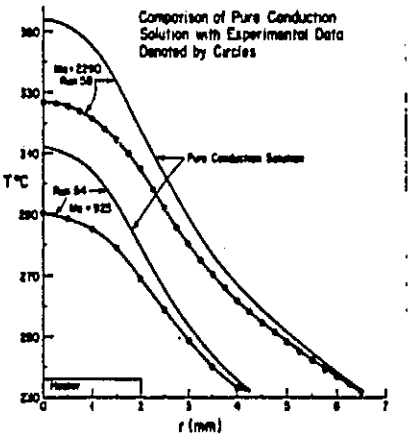

Fig. 8. Comparison of pure conduction solution with experimental data.

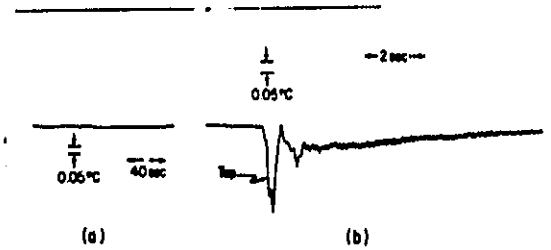

Fig. 9. (a) Recorder trace of thermocouple #1 with 2ℓ = 11.7 mm and T_c = 166°C.
(b) Response of thermocouple output to a mechanical tap on the system.

Minimum amplitude detection limit. Figure 9 presents a recorder trace from the experiment which demonstrates the amplitude sensitivity of the experimental system. We estimate that oscillations of amplitude greater than or equal to 0.4 μV would be detectable if present in the signal. For the type K thermocouple used here, this would correspond to 0.01°C. The ability of the system to detect temperature oscillations was qualitatively confirmed by giving the system a sharp mechanical tap with the result shown in Fig. 9b. Furthermore, the attenuation of the oscillations produced by tapping the system indicates its stability to finite amplitude perturbations.

Frequency response. The expected frequency of Marangoni induced oscillatory flow in low Prandtl number systems in the disk geometry is unknown. If the frequency were high, the

limited time response of our recording system would reduce the amplitude of the measured oscillation. The time response of our recorder was evaluated by measuring the decrease in amplitude of a sine wave supplied by a frequency generator as a function of frequency, utilizing the same scale as in the experiment. In addition to limitations resulting from the recorder, one must also consider the loss of amplitude due to the finite time response of the thermocouple itself. The time constant of a 0.25 μm diameter thermocouple, τ, has been measured /4/ in molten Sn-Pb alloys to be 35 ms. The fractional drop in amplitude as frequency, f, increases can be taken /5/ as, $1/(1 + (2\pi f)^2)^{1/2}$. The total fractional loss of amplitude was taken as the product of that due to the recorder and the thermocouple, and the results show that the minimum detectable amplitudes of the temperature oscillations are 0.01, 0.013, 0.062, 0.34 and 3.15°C for frequencies of 0.1, 1, 5, 10 and 20 Hz. Thus, temperature oscillations of amplitudes greater than 0.5°C could have been present in the tin disks and would not have been detected if their frequencies were above around 10 Hz.

Cleanliness of molten tin surface. In previous work /6/, we have shown that one may utilize LEEL spectroscopy with the cylindrical mirror Auger analyser to detect tin oxide layers on molten tin of less than a monolayer. By utilizing this technique, coupled with Auger spectroscopy to evaluate other surface contaminants, the following picture emerged. The original tin surface was carefully electropolished. Before the initial melting at a pressure of less than 10^{-9} Torr, the surface was contaminated by a very thin C layer on top of tin oxide. When this contamination was removed by sputtering before melting, it was found that upon melting the molten surface became contaminated with both oxygen and sulfur. These contaminates could be removed by moving the argon sputter beam over the molten surface, and the surface would remain clean over 12 hour periods.

However, if the power were increased to melt out to a larger zone radius, the surface became contaminated again. Obviously, oxygen and sulfur impurities in the solid tin contaminated the surface upon melting. We were never able to clean the surface completely out to the full molten zone radius, perhaps due to surface diffusion. By moving the sample under the Auger analyser, it was determined that at the maximum molten zone diameter of 11.7 mm, the central 10.4 mm was atomically clean, but an outer annulus of 0.65 mm width was covered with a few monolayers of contaminant. It seems doubtful that this small amount of contamination would affect the Marangoni flow, particularly since the maximum temperature gradients occur in the atomically clean part of the zone.

Evaluation of Marangoni and Reynolds numbers. Schwabe, et al. /1/ have presented careful experimental studies which detect the onset of oscillatory flow in $NaNO_3$ (Pr = 9) at a Ma number of about 7400. Although these experiments utilized a different geometry than was used here, and a fluid with a much higher Pr number, they present a useful guide for these studies.

In order to evaluate Ma, the velocity and temperature distributions in the DFZ geometry used here were computer modeled with our finite difference techniques, and we found Ma = 4300 for this experiment. Previous work with $NaNO_3$ disks showed this approach is effective /7/. It might be noted that one could evaluate Ma more directly from experimental data by moving the thermocouple to the center of the molten disk. This was done on initial experiments, and agreement of the Ma values determined by both techniques was good. In the present experiment, the thermocouple located at r = 3 mm, because it was felt that the amplitude of temperature oscillations would be higher there than at the center position.

CONCLUSIONS

Mathematical models of Marangoni flow in a tin disk heated from below indicate the flow has a two cell structure in which one cell is a thin surface boundary layer which decreases in thickness as the parameter $(d/\ell)^3 Ma/Pr$ increases. Finite difference calculations give radial distribution of surface velocity which exhibits double peaks as the Marangoni number increases.

Experiments, in which the surface of the thin molten tin disk was atomically clean, show no evidence of thermal or hydrodynamic oscillations in the melt at Marangoni numbers up to 4300. The effect of natural convection in these experiments was very small because the Bond number, $d^2 g\beta\rho/|d\sigma/dT|$, was kept below approximately 0.05 by maintaining d less than or equal to 0.12 cm.

ACKNOWLEDGEMENT

This work was supported in part by a grant from NASA.

REFERENCES

1. D. Schwabe, F. Preisser and A. Scharmann, J. Fluid Mech., 126, 545 (1983), J. Crystal Growth, 52, 435 (1981).

2. D. Chun and A. Scharmann, J. Crystal Growth, 46, 125 (1979).

3. Ch. H. Chun, Acta Astranautica, 7, 479 (1980).

4. J. Nanigan, Nanmac Temperature Handbook, p. L27, Nanmac Corp., Framingham, MA (1981/82).

5. R.P. Benedict, Fundamentals of Temperature, Pressure and Flow Measurement, p. 270, John Wiley, NY (1977).

6. A.J. Bevolo, J.D. Verhoeven and M. Noack, Surface Science, 134, 499 (1983).

7. C.C. Hsu, W.N. Gill, M.A. Noack and J.D. Verhoeven, Chem. Engr. Comm., 24, 289 (1983).

II. Paper presented at Symposium on Chemical and Physical Processing of Integrated Circuits, to be published in A.C.S. Symposium Series, (1984 or 85).

CONVECTIVE DIFFUSION IN ZONE REFINING OF LOW PRANDTL NUMBER LIQUID METALS AND SEMICONDUCTORS

by
William N. Gill*, Nicholas D. Kazarinoff**
and John D. Verhoeven†

*Chemical Engineering Department, **Mathematics Department,
State University of New York at Buffalo, Amherst, NY 14268 and
†Materials Science and Engineering Department,
Iowa State University, Ames, IA 50011

Several elementary aspects of mass diffusion, heat transfer and fluid flow are considered in the context of the separation and control of mixtures of liquid metals and semiconductors by crystallization and float-zone refining. First, the effect of convection on mass transfer in several configurations is considered from the viewpoint of film theory. Then a nonlinear, simplified, model of a low Prandtl number floating zone in microgravity is discussed. It is shown that the nonlinear inertia terms of the momentum equations play an important role in determining surface deflection in thermocapillary flow, and that the deflection is small in the case considered, but it is intimately related to the pressure distribution which may exist in the zone. However, thermocapillary flows may be vigorous and can affect temperature and solute distributions profoundly in zone refining, and thus they affect the quality of the crystals produced.

Introduction

The basic idea of zone refining is that a liquid region or zone is created by melting a small fraction of the material in a relatively long solid charge, ingot or feed stock. By moving this liquid zone through the charge in one direction the solid phase can be purified as the forward surface is melting and the rear one solidifies. This is referred to as zone refining. If the liquid zone is passed through the charge in both the forward and reverse directions, a uniform distribution of impurities may be obtained. This is zone leveling.

Pfann (1) first described the essential features of zone refining and pointed out its potential as a separation technique. In the early 1950's it was used to provide high purity silicon and germanium for semiconductor applications. Since then it has been used in a variety of applications. The real power of zone refining is that one can pass a molten zone through a solid phase numerous times without difficulty. Up to a limit each pass increases the purity of the solid phase by decreasing the concentration of the solute. It is by means of multipass operation that great purity can be achieved in the solid phase.

Zone refining is a dynamic nonequilibrium separation process. However, to understand its essential features it is important to understand the equilibrium concepts on which it is based. Of central importance is the notion of the equilibrium distribution coefficient, $k_o = C_S/C_L$, where C_S and C_L are the concentrations of solute at equilibrium in the solid and liquid phases respectively. Since the value of k_o may be dramatically different from unity, it is clear that at equilibrium a solute may distribute itself between solid and liquid phases with a great preference for one or the other at a given temperature. On this basis the relative amount of solute in each phase can be controlled, and a separation can be carried out.

Phase diagrams, which describe the equilibrium relations that exist between phases in mixtures, are often very complex as is the case with the nickel-aluminum diagram for example. However, if one restricts attention only to a relatively narrow range of concentration and, in particular, to dilute solutions, then one can simplify this description of these relationships markedly by using straight line approximations as shown in Figures 1(a, b).

Figures 1(a, b) represent phase relationships for cases in which solid solutions exist, a common occurrence in metallic and semiconductor systems. In such cases solidification does not cause complete separation and the degree of separation depends not only on the equilibrium relationships represented by Figures 1(a, b) but

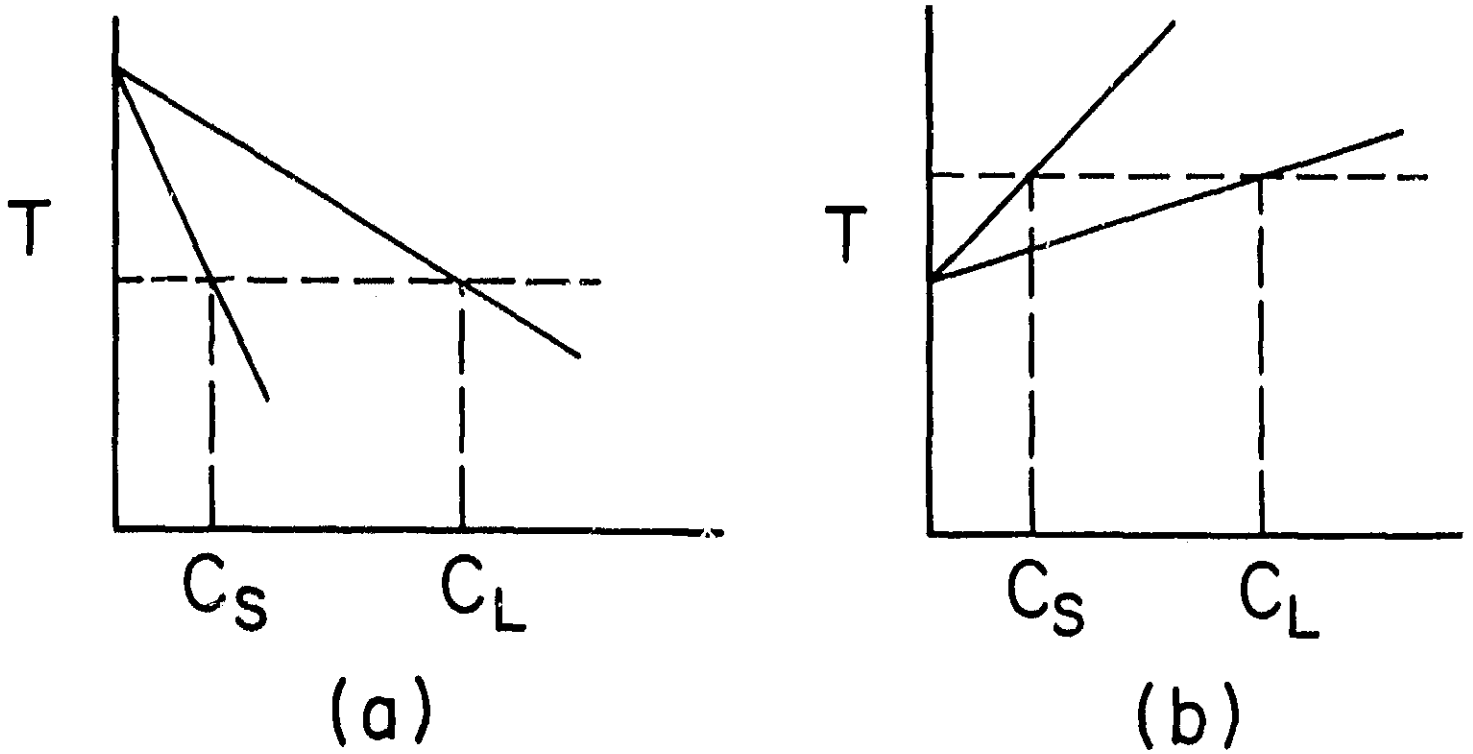

Figure 1. Possible solid-liquid phase diagrams.

also on the convective-diffusive characteristics of the system. If the addition of solute lowers the melting point as in Figure 1a, then $k_o < 1$; on the other hand if the melting point is raised by adding solute, $k_o > 1$ as in Figure 1b.

A solute distribution exists in the melt because the solidification is carried out at a finite rate. For example, if $k_o < 1$, then solute is rejected and accumulates at the surface which is solidifying, and this creates solute gradients in the melt which tend to be relaxed by molecular diffusion and any convection which may exist. The interfacial distribution coefficient, k, refers to the solid to liquid solute concentration ratio at the interface. It is k which is used in transport calculations when one is trying to understand the dynamic behavior of zone refining systems. It usually is found that equilibrium exists locally at the solid-liquid interface, in which case $k = k_o$.

The concentration, C_L, of solute in the liquid in the neighborhood of the solid-liquid interface is strongly influenced by k which thereby affects the concentration in the solid phase after solidification in at least two ways. First, the smaller k is the faster solute will accumulate on the liquid side of the interface. Second, it is the value of $C_L(0)$ which determines C_S at the interface for a given value of k. With no convection in the melt, it will be shown that the maximum interfacial concentration is approached as

the process progresses and is, $C_L(0) = C_L(\infty)/k$, where $C_L(\infty)$ is the concentration of solute in the solution outside the diffusion boundary layer. $C_L(0)$ climbs from $C_L(\infty)$ to the $C_L(\infty)/k$ asymptote.

The material to be purified often is very reactive, and it is difficult to find container materials which it will not attack. In such cases floating-zone melting is attractive and is used for example to grow oxygen free silicon crystals. In this case the molten zone is held in place by its own surface tension which works against the action of gravity. A molten zone can be established between two rods, one a polycrystalline charge or feed rod and the other a crystalline rod of purified material which is either the product of the separation or may serve as the feed for another pass. The molten zone may be created in several ways including radio-frequency induction heating as is used for silicon or electron beam heating which is favored for refractory materials.

The gravitational field limits the length of the molten zone that can be sustained by surface tension forces, and this also limits the crystal diameter. The possibility of reducing these constraints by decreasing significantly the intensity of the gravitational field has generated considerable interest in performing floating zone experiments in an orbit around the Earth.

Heating from an external source creates rather large temperature gradients along the surface of the floating zone which give rise to strong thermo-capillary convective flow which mixes the melt. Furthermore this flow may couple with natural convection flows driven by the gravitational field. These flows give rise to time-dependent behavior which is of considerable theoretical and practical interest because it creates growth striations in semiconductor crystals which affect their performance, and because its origin, and the parameters which characterize it, are not well understood.

A detailed review of zone melting and its applications has been given recently by Shaw (2). In the present paper we shall confine our attention primarily to the convective-diffusive characteristics of such systems, and we shall strive primarily to obtain a sound qualitative understanding of their behavior.

The flow phenomena involved in zone refining will be discussed briefly. In particular we shall consider surface tension driven flow in a cavity containing a low Prandtl number, Pr, fluid (a low Pr number is typical of liquid metals and semiconductors). It will be shown that simplified models of such flow, which simulate the melt configuration in zone refining, predict multiple steady-state solutions to the Navier-Stokes equations exist over a certain range of the characteristic parameter.

The Equations of Motion, Energy and Diffusion for Molten Zones

In actual zone refining operations one may encounter three-dimensional simultaneous heat and mass transfer with moving interfaces, and the system also may be time dependent. The mode of heating affects system behavior significantly, as does radiation, when materials with high melting points are involved. All of these factors complicate the analysis of the diffusional aspects of this separation process. Therefore we shall treat some rather simplified

versions of real systems in an effort to gain some insight into several of the important phenomena which occur.

First, we shall assume the system is two-dimensional and that the physical properties, except surface tension and density (in the body force term of the momentum equations) are constant. With these assumptions the continuity equation, momentum equations, energy equations and the diffusion equation are given by

$$\frac{\partial u}{\partial x} + \frac{\partial v}{\partial y} = 0 \tag{1}$$

$$\frac{\partial u}{\partial t} + u\frac{\partial u}{\partial x} + v\frac{\partial u}{\partial y} = -\frac{1}{\rho_\infty}\frac{\partial P}{\partial x} + \upsilon\left[\frac{\partial^2 u}{\partial x^2} + \frac{\partial^2 u}{\partial y^2}\right] + \frac{\rho}{\rho_\infty} g_x \tag{2}$$

$$\frac{\partial v}{\partial t} + u\frac{\partial v}{\partial x} + v\frac{\partial v}{\partial y} = -\frac{1}{\rho_\infty}\frac{\partial P}{\partial y} + \upsilon\left[\frac{\partial^2 v}{\partial x^2} + \frac{\partial^2 v}{\partial y^2}\right] + \frac{\rho}{\rho_\infty} g_y \tag{3}$$

$$\frac{\partial T}{\partial t} + u\frac{\partial T}{\partial x} + v\frac{\partial T}{\partial y} = \alpha\left[\frac{\partial^2 T}{\partial x^2} + \frac{\partial^2 T}{\partial y^2}\right] \tag{4}$$

$$\frac{\partial C}{\partial t} + u\frac{\partial C}{\partial x} + v\frac{\partial C}{\partial y} = D\left[\frac{\partial^2 C}{\partial x^2} + \frac{\partial^2 C}{\partial y^2}\right]. \tag{5}$$

The boundary conditions for Equations 1-5 depend on the mode of heating and the way the separation is conducted. To gain some insight into how the separation occurs at the solid-liquid interface we first consider Equation 5. We shall assume that the melt is quiescent so that the process is governed entirely by diffusion and u and v are zero. If there is no convection in the melt and directional solidification is occurring only in the x-direction, then Equation 5 becomes

$$\frac{\partial C}{\partial t} = D_L \frac{\partial^2 C}{\partial x^2}. \tag{6}$$

Let us now assume, as is customary, that the charge is being moved through the heater at a constant velocity U, and that this causes the solid-liquid interface to move at the velocity U. Then it is convenient to use a coordinate X which moves with the interface such that

$$X = x - Ut \tag{7}$$

and Equation 6 becomes

$$\frac{\partial C}{\partial t} - U\frac{\partial C}{\partial X} = D_L\frac{\partial^2 C}{\partial X^2}. \qquad (8)$$

At time $t = 0$ the solute concentration in the charge was C_o. Since diffusion in the liquid phase is slow, we can assume the diffusion layer near the interface is thin compared to the length of the melt; and therefore $C(t,\infty) = C_o$. Now we must consider the boundary condition at the interface. To do this we equate the fluxes in the solid and liquid phases at $X = 0$ and remember that with respect to X there is an apparent convective velocity equal to $-U$. Furthermore, $D_L >> D_S$ so that solid phase diffusion can be neglected. Therefore

$$-\frac{\partial C}{\partial X}(t,0) = \frac{(1-k)\,U}{D_L}C(t,0), \qquad (9)$$

where $k = \dfrac{C_S(t,0)}{C_L(t,0)}$. If we assume $k = k_o$ and use the idealized phase diagram with straight lines shown in Figure 1, k is constant and this makes it much easier to solve the problem posed in Equation 8 and 9 together with the other initial and boundary conditions.

Order of Magnitude Considerations

There are various ways of using Equations 8 and 9 to obtain information about the solidification process. The simplest one is to do an order of magnitude analyses, OMA, of these equations. This yields immediately that on a relative basis the first, second and third terms are of order $1/t$, U/δ and D_L/δ^2, where δ is the approximate thickness of the diffusion boundary layer. Equating the first and last terms gives

$$\delta \sim \sqrt{D_L t}, \qquad (10)$$

and the second and last terms give

$$\delta \sim D_L/U. \qquad (11)$$

A similar OMA of Equation 9 yields

$$\frac{C(0)}{C_o} \simeq \frac{1}{1 - (1-k)\,\frac{U\delta}{D_L}}. \qquad (12)$$

If one combines Equations 10, 11 and 12, one gets

$$\frac{C(0)}{C_o} = \frac{1}{1 - (1-k)\ tU^2/D_L}, \qquad t << \frac{D_L}{U^2}, \tag{13}$$

and

$$\frac{C(0)}{C_o} = \frac{1}{k}, \qquad t >> \frac{D_L}{U^2}. \tag{14}$$

Equations 13 and 14 provide a qualitative picture of the relationship between the concentration at the solid-liquid interface and that in the bulk of the melt.

We see from Equations 10-14 that two time regimes exist in the problem. The first period is a transient period which exists at $t << D_L/U^2$. The second period is a steady state one which occurs when $t >> D_L/U^2$. Since D_L is a physical property which cannot be manipulated, we see that the greater the velocity of solid-liquid interface the more quickly a steady state is reached in the system. This conclusion is of practical importance because one often wishes to distribute the solute throughout the solid with a constant concentration.

Exact One-Dimensional Solutions of Diffusion Equation

In the steady state $\partial C/\partial t = 0$, and Equations 8 and 9 can be solved easily to give

$$C_L/C_o = 1 + \frac{1-k}{k} \exp\left(-\frac{UX}{D_L}\right), \tag{15}$$

which gives the steady state solution for the interfacial concentration as

$$\frac{C_L(0)}{C_o} = \frac{1}{k}. \tag{16}$$

Equation 16 shows clearly that the solid phase steady concentration is C_o, the initial melt concentration. It is interesting to note that Equations 14 and 16 are identical.

The solution of Equation 8, if one includes the unsteady state effect is more complex, and was apparently first shown by Smith et al. (3) to be,

$$\frac{C_L}{C_o} = 1 - \frac{1}{2}\left\{\operatorname{erfc}\frac{X+Ut}{2\sqrt{D_L t}} + \frac{hD_L}{hD_L - U} e^{\frac{-UX}{D_L}} \operatorname{erfc}\frac{X-Ut}{2\sqrt{D_L t}}\right.$$

$$+ \frac{U-2hD_L}{2(U-hD_L)} e^{-hX + ht(hD_L-U)} \operatorname{erfc} \frac{X+(U-2hD_L)t}{2\sqrt{D_L t}}\}, \qquad (17)$$

where $h = (1-k)U/D_L$.

Equation 17, evaluated at $X = 0$, together with the definition of k, and setting $t = x/U$, enables one to calculate the solid phase distribution as

$$\frac{C_S}{C_o} = \frac{1}{2}\{1 + \operatorname{erf}\sqrt{\frac{Ux}{4D_L}} + (2k-1) \exp[-k(1-k)\frac{Ux}{D}] \operatorname{erfc}[(2k-1)\sqrt{\frac{Ux}{4D_L}}]\}, \qquad (18)$$

where x is the distance from the point at which the first solid was frozen.

Effect of Convection on Segregation

The preceding discussion assumes that no convection exists in the melt, and this is rarely, if ever, the case. Next we shall consider two approaches which account for convection in the melt, a transport mechanism which is especially important in mass transfer because D_L is small and even weak convection markedly alters solute concentration profiles and may cause macrosegregation. First we shall discuss film theory which is a very simple approach that gives qualitative information and often provides considerable physical insight into the mechanisms involved. Second, we shall discuss a simplified model of zone refining.

In film theory one assumes that the concentration changes near the interface occur in a very thin region of thickness δ. In this region the differential equation which describes the concentration is given by the steady state $(\frac{\partial C}{\partial t} = 0)$ form of Equation 8. The magnitude of δ is determined by the convection which exists in the system. One estimates δ by solving simplified convection problems such as natural or forced convection along a flat surface, or two or three-dimensional stagnation flow, etc. From these simple cases one calculates the mass transfer coefficient, k_m, and δ is defined as $\delta = D_L/k_m$. In essence, one neglects all convection when calculating C in the stagnant film, and includes all convective effects in its thickness, δ. The stronger the convection the smaller is δ.

The steady-state solution satisfying Equations 8 and 9 and $C = C_0$ at $X = \delta$ is

$$\frac{C}{C_o} = \frac{k + (1-k)\, e^{-\frac{U}{D_L}X}}{k + (1-k)\, e^{-\frac{U}{D_L}\delta}}. \qquad (19)$$

Therefore, one obtains the well known Burton-Prim-Slichter (4) equation

$$\frac{C_S}{C_o} = \frac{k}{k + (1-k)e^{-\frac{U}{D_L}\delta}}, \tag{20}$$

and the problem is reduced to choosing an expression for δ which represents a realistic estimate of the convective patterns which exist in the melt. Let us use a few relevant examples to illustrate how film theory may be applied to zone refining.

By definition, the mass transfer coefficient is given by

$$j = -D_L \frac{\partial C(0,y)}{\partial x} = k_m(C(0) - C_o),$$

where y is the distance parallel to the surface and x is normal to it. Therefore the definition of δ is,

$$\delta = \frac{D_L}{k_m} = \frac{C(0) - C_o}{-\frac{\partial C}{\partial x}(0,y)} = \frac{y}{Sh_y},$$

where Sh_y is the Sherwood number defined by $\frac{k_m y}{D_L}$ and $\frac{\partial C(0,y)}{\partial y}$ is calculated from a problem similar to the one to which we are applying film theory, but one that can be analyzed more easily. For example, to calculate $\frac{\partial C(0,y)}{\partial x}$, one would not include the moving boundary because that is included in the film model, the steady state form of Equation 8. One might also use a constant concentration or constant gradient boundary condition at the interface rather than Equation 9 which also is included in the film model.

Suppose natural convection is the dominant convection mode in the melt. If a natural convection boundary layer created by concentration gradients exists, then its behavior depends on whether the interface is vertical or horizontal to the earth. If it is vertical, one can show that,

$$Sh_y = 0.54\ Ra_y^{1/4} = 0.54\left(\frac{\beta g \Delta C y^3}{\nu D_L}\right)^{1/4} \tag{21}$$

may be a reasonable approximation, Kays and Crawford (5), and

$$\delta \cong \frac{1}{0.54}\left(\frac{\nu D_L y}{\beta g \Delta C}\right)^{1/4}. \tag{22}$$

If it is horizontal, Stewartson (6) and Gill et al. (7) showed that

$$Sh_y \simeq 0.75\ Ra_y^{1/5} \tag{23}$$

may apply if the interface faces upward and the density of the fluid adjacent to it increases with distance from the interface; or if it faces downward and the density relationship is reversed. In this case

$$\delta \simeq \frac{4}{3}\left(\frac{\nu D_L y}{\beta g \Delta c}\right)^{1/5} . \tag{24}$$

The important point made by Equations 20, 22 and 24 is that δ is a function of y, the distance parallel to the interface, and this leads to segregation in the y direction (a nonuniformity of solute concentration) in the solid phase as given in Equation 20.

It is most desirable for δ to be constant, and there are ways to make this happen. If the solid-liquid interface is circular, which is most often the case because the charge is a rod, then δ can be controlled by rotating the rod so that the interface behaves as a rotating disk with angular velocity ω. This configuration is widely used in analytical and electrochemistry because δ is essential constant if this mechanism controls. Levich (8) has shown that for a rotating disk

$$\delta = 1.61\left(\frac{D_L}{\nu}\right)^{1/3}\sqrt{\nu/\omega}. \tag{25}$$

Equation 25 shows that δ is constant and its magnitude can be controlled by changing ω.

Natural convection to blunt bodies such as cylinders (2-dimensional) and spheres (3-dimensional) has been studied by Acrivos (9) and from his analysis one can show that these configurations are characterized by constant boundary-layer thicknesses. For 2-dimensional bodies,

$$\delta = \frac{1}{0.54}\left(\frac{R\ \nu D_L}{\beta g \Delta C}\right)^{1/4} , \tag{26}$$

and for 3-dimensional ones,

$$\delta = \frac{1}{0.54(2)^{1/4}}\left(\frac{R\ \nu D_L}{\beta g \Delta C}\right)^{1/4} , \tag{27}$$

where R is the radius of curvature of the surface. Note that Equation 26 is identical to 22 except that the length scale is R which is a constant, and thus δ is a constant. This implies that the interfacial concentration of solute is uniform across the stagnation region. These results may apply to an interface which faces downward (in the direction of the gravity vector) into a fluid whose density increases with distance from the interface or one

which faces upward into a fluid of decreasing density with distance from the interface.

When strong temperature gradients exist, natural convection may be primarily induced thermally or both heat and mass transfer may play comparable roles. In these cases the situation is more complex, because the number of parameters increases. In liquid metals and semiconductors the Schmidt number, ν/D_L, is several orders of magnitude greater than the Prandtl number, ν/α, and this enables one to solve for the concentration profile in a rather general way without great difficulty as will be discussed next.

The number of alternative configurations of the melt and modes of heating it that may exist in zone refining is very large. Therefore it seems desirable to have a method which enables one to estimate macrosegregation under a wide variety of flow conditions. Such an approach is not available now, but some progress toward it can be made by noting that liquid phase diffusion is characterized by a large Schmidt number, which implies that diffusion boundary layers are thin compared to momentum boundary layers. It seems that Lighthill (10) was the first to suggest that one can restrict attention to the velocity field near the interface under these conditions, and by doing this one can derive the expression

$$\delta = 0.894\left(9D_L\mu\right)^{1/3}\tau_w^{-1/2}\left[\int_o^y \tau_w^{1/2}\,dy\right]^{1/3}. \qquad (28)$$

Equation 28 is a general result for high Sc, two-dimensional flows in which the diffusion boundary layer thickness is zero at $y = 0$. It includes Equations 22 and 24 as special cases, but it does not apply to systems in which $\delta \neq 0$ at $y = 0$, such as stagnation regions, and also it does not include Equation 25. Equation 28 can be applied to flows which are driven by temperature differences regardless of the magnitude of the Prandtl number.

To use Equation 28 for thermally driven free convection boundary layers one simply calculates $\tau_w = -\mu\,\frac{\partial u(0,y)}{\partial x}$ from known solutions. Then this result is inserted in Equation 28 and δ in Equation 19 or 20.

Unfortunately, because of the variety of factors, such as shape, mode of heating and orientation, that is possible in melts, and the complexity of the flow patterns which may exist, it is extremely difficult to offer general rules, a priori, on how to estimate δ. One needs to examine each particular case carefully to obtain even a qualitative understanding of the macrosegregation that may occur in the crystals being produced. However, one procedure which seems to yield generally beneficial results is crystal rotation as predicted by Equation 25.

Simplified Model of Surface Tension Driven Flow in a Two-dimensional Molten Zone Supported on the Bottom

The preceding discussion showed that steady-state natural convection often leads to undesirable macrosegregation. It also has been shown by Gill (11) that natural convection flows may become unstable, and Carruthers (12) and Milson and Pamplin (13) have discussed the

implications of the resulting oscillations on crystal growth. In this section we shall examine exact solutions of the Navier-Stokes equations for a two-dimensional simplified model of a molten zone which is in the form of a cavity or slot of liquid, of depth d, supported on the bottom, but with a free surface on top. The zone is heated over the length, $-\ell < x < \ell$, by a flux, q, and cooled on its ends at $x = \pm L$, where $L > \ell$. We shall study the core region inside $-\ell < x < \ell$ for which a similarity solution exists. Thus we are neglecting end-effects.

One can show that Equation 4 is satisfied by a temperature distribution in the form

$$\Theta = \frac{T - T_{cold}}{T_{hot} - T_{cold}} = g_1(\eta) + g_2(\eta)\left(\frac{x}{\ell}\right)^2, \tag{29}$$

where g_1 and g_2 are functions which are determined from

$$g_1'' + 2A^3 Ma\, f\, g_1' = -2A^2 g_2 \tag{29a}$$

and

$$g_2'' + 2A^3 Ma\left[f\, g_2' - f'\, g_2\right] = 0 \tag{29b}$$

with the initial conditions

$$g_1'(0) = g_2'(0) = 0 \tag{29c}$$

$$g_1(0) = -g_2(0) = 1, \tag{29d}$$

and $\eta = y/d$. Here $f(\eta)$ and $f'(\eta)$ are functions related to u and v which will be determined later; Ma is the Marangoni number $\frac{\Delta T\, \ell \left| d\alpha/dT \right|}{\mu\alpha}$; and A is the aspect ratio $\frac{d}{\ell}$. In the limit $Pr \to 0$, the solution given by solving Equations 29 implies a constant heat flux along the bottom of the cavity, $\eta = 1$, and a zero heat flux from the free surface, $\eta = 0$, into the vacuum surrounding the liquid zone. For non-zero Pr the flux at $\eta = 1$ varies with x. Obviously Equation 29 implies that the liquid surface temperature varies as

$$T(x,0) = T_h - (T_h - T_c)\left(\frac{x}{\ell}\right)^2 = T_h - \Delta T x_1^2, \tag{29e}$$

where T_h is the temperature at $x = 0$ and T_c is that at $x = \pm\ell$. Gill et al. (14) have shown by numerical computation that Equation 29e is a good approximation to a constant heat flux for fluids with finite values of Pr which are typical of liquid metals. Therefore the following discussion applies best to low Pr fluids, a category that includes essentially all fluids of interest in semiconductor technology as well as all liquid metals. On the other hand, the most complete data on thermocapillary flows in molten zones has been

reported by Preisser, Scharmann and Schwabe (15) and Schwabe and Scharmann (16) for $NaNO_3$ which has a Prandtl number of 9 and for heating from the side which is not consistent with the present theory.

Levich (8) has discussed capillary motion in two-dimensional creeping flows in which the surface was flat. Yih (17) pointed out inconsistencies in Levich's analysis which were associated with the assumptions of a linear distribution of surface tension with distance along the interface, and with the deflection of the surface which inevitably occurs when capillary flow exists. He noted that under certain circumstances steady flows may not exist. Ostrach (18, 19) has discussed scaling problems in capillary flows. Recently, Sen and Davis (20) studied capillary flow in bounded cavities in which d/ℓ is small, end effects are present, and the flow is very slow and the cavity is heated from the side. Cowley and Davis (21) studied the high Marangoni number "Thermocapillary analogue" of a buoyancy driven convection problem solved by Roberts (22). Later, we shall make some comparisons between our results for the deflection of the surface and those of Sen and Davis (20).

The boundary conditions for Equations 1-3 which will be satisfied at $x = 0$ and the solid bottom are straightforward, but those for the free surface are rather complex and call for some discussion. At $x = 0$ we have a stagnation condition and at $y = d$ there is no slip and no penetration of fluid through the solid bottom. Therefore

$$u(x, d) = v(x, d) = 0, \quad (0 \leq x \leq \ell) \text{ and } u(0, y) = 0, \quad (0 \leq y \leq d) \tag{30}$$

The free surface is not flat in general and the boundary conditions on this surface require careful consideration. The kinematic condition at $y = -h(x)$, where $h(x)$ is the deflection from the flat surface at $y = 0$, is

$$v(x, -h) = -\frac{dh}{dx}\, u(x, -h). \tag{31a}$$

Equation 31a is the steady state form of the kinematic condition which also is used to describe wave motion as discussed on page 595 of Levich's book, Physicochemical Hydrodynamics. One also must equate the normal and tangential components of the forces in each phase at the free surface. Since we consider a gas-liquid interface, we neglect gas phase resistance due to its viscosity and include only the pressure it imposes on the interface on the gas side. Therefore, at $y = -h(x)$ the tangential component of the stress tensor for the liquid phase is equal to the tangential force created by the change in surface tension with temperature in the x direction. Thus the tangential force balance at the interface becomes

$$\frac{-\mu}{1 + h_x^2}\left[(1-h_x^2)\left(\frac{\partial u}{\partial y} + \frac{\partial v}{\partial x}\right) - 2h_x\left(\frac{\partial v}{\partial y} - \frac{\partial u}{\partial x}\right)\right] = \frac{\sigma_x}{(1 + h_x^2)^{3/2}}, \tag{31b}$$

and the normal force balance becomes

$$-(p-p_g) + \frac{2\mu}{(1+h_x^2)}\left[\frac{\partial v}{\partial y} + h_x\frac{\partial u}{\partial y} + h_x\left(\frac{\partial u}{\partial x}h_x + \frac{\partial v}{\partial x}\right)\right] = \frac{\sigma h_{xx}}{(1+h_x^2)^{3/2}}, \quad (31c)$$

where σ is the surface tension and the x-subscripts on h and σ denote differentiation with respect to x, and p_g is the pressure in the gas phase over the liquid which at zero g is taken to be zero.

To solve Equations 1-3 together with 30 and 31a-c we take note of the important role played by the surface tension number, $\varepsilon = \frac{\mu\nu}{d\sigma_o}$, where σ_o is the surface tension at temperature T_o. In the liquid metal and semiconductor systems we are considering ε is very small (i.e. $\varepsilon \approx 10^{-7}/d$ for liquid tin); therefore a first order perturbation solution in ε should be adequate. Consequently we introduce a stream function, ψ and a similarity coordinate, η, so that Equations 1-3, 30 and 31a-c are satisfied to $O(\varepsilon)$, and the computations are reduced to solving a two-point-boundary-value problem for a single nonlinear ordinary differential equation in the dimensionless stream function f. The procedure for finding the base flow solution, which is equivalent to finding f and η for $\varepsilon = 0$, is similar to that employed by Carter and Gill (23) to treat the entirely different physical problem of flow with heat transfer, blowing or suction, and natural convection in flows between parallel-plates or in tubes. As usual we define

$$u = \frac{\partial \Psi}{\partial y}, \quad -v = \frac{\partial \Psi}{\partial x}. \quad (32)$$

We choose $\eta = y/d$ which suggests

$$\Psi = U_R(x)\, d \int_o^\eta \frac{u(x,y)}{U_R(x)}\, d\eta.$$

If $u(x,y)$, scaled by $U_R(x)$, is a function of η only, then

$$\Psi = U_R(x)\, d\, f(\eta). \quad (33)$$

Equations 2, 32 and 33 lead to

$$f''' + \frac{d^2}{\nu}\frac{dU_R}{dx}\left(ff'' - f'^2\right) = \frac{d^2}{\mu U_R}\frac{\partial p}{\partial x} = \beta \quad (34)$$

which satisfies Equations 1-3 exactly. Clearly the coefficient $\frac{d^2}{\nu}\frac{dU_R}{dx}$ is constant, and Equation 31b is satisfied, if

$$U_R = \frac{2\left|\frac{d\sigma}{dT}\right| \Delta T d}{\mu \ell} \left(\frac{x}{\ell}\right) \qquad (34a)$$

so that

$$u = 2(\nu/d)\, A^2 Re\, x_1\, f'(\eta),\quad v = -2(\nu/d)\, A^3\, f(\eta). \qquad 35(a,b)$$

where $x_1 = x/\ell$ and $A = d/\ell$. To obtain Equation 34a we use Equation 29 and $\sigma = \sigma_o + \frac{d\sigma}{dT}(T-T_o)$ which yields $\sigma/\sigma_o = 1 + ARe\varepsilon\, x_1^2$. Equation 34 then becomes

$$f''' + 2\left(\frac{d}{\ell}\right)^3 \frac{Ma}{Pr}(ff'' - f'^2) = \beta, \qquad (36)$$

and the boundary conditions become

$$f(0) = f(1) = f'(1) = f''(0) + 1 = 0, \qquad (37)$$

where $\frac{Ma}{Pr} = Re = \frac{\Delta T \ell \left|d\sigma/dT\right|}{\mu\alpha}\left(\frac{\alpha}{\nu}\right)$ and the last boundary condition given by Equation 37 is obtained by substituting Equations 32a,b into Equation 31b which is satisfied to $O(\varepsilon)$. Since Equation 36 is of third order and 37 includes four boundary conditions, the constant β can be determined as a function of $Q = 2\left(\frac{d}{\ell}\right)^3 \frac{Ma}{Pr}$, and the solution for f can be related to u and v via Equations 32 and 33. An important feature of Equation 36 is that it retains the essential nonlinear features of the Navier-Stokes equations. It will be seen later that the nonlinear terms are of great importance even at relatively small values of Q, and it is they which determine if multiple solutions to Equation 36 do exist.

Brady and Acrivos (24) studied an entirely different physical problem with different boundary conditions from those given in Equation 37 and cautioned that the numerical solutions they obtained for a system with a capped end differed from the similarity solutions. Their problem differs fundamentally from the present one in several ways. First, the flow in our problem is symmetric about $x = 0$, because surface heating is symmetric about $x = 0$ over the region $-\ell < x < \ell$, and this causes $u = 0$ at $x = 0$. Hence, our solution is exact near $x = 0$. Their problem is antisymmetric about $x = 0$, and they apparently have a "collision region" near $x = 0$ which affects the structure of the entire flow. Second, Brady and Acrivos specify the shape of their cavity, $h(x)$, as part of the problem statement, and their choice of shapes may be inconsistent with the pressure distribution in their similarity solutions which

they use as the criterion for agreement with their numerical calculations. We solve for the shape of the zone and require it to be consistent with the pressure distribution to $O(\varepsilon)$ in Equation 31c. Third, the shape of the zone affects the boundary conditions on v through the kinematic condition, and therefore our boundary conditions are different from theirs. Furthermore, Gill et al. (14) found good agreement between similar solutions for thermocapillary flow in an infinite disk and numerical solutions to a finite disk with end effects. In the thermocapillary problem (14) the boundary conditions were identical to those in Equation 37.

We studied the two-point-boundary-value problem (TPBVP) Equations 36 and 37 (corresponding to a slot with one free surface) by suspending the trivial differential equation

$$\beta' = 0 \tag{38}$$

to 36 and using the TPBVP solver BOUNDS, P. Deuflhard (25), to solve the resultant well-posed problem, Equations 36, 37 and 38. BOUNDS is an accurate, multiple-shooting code. We began with the solution

$$f = \eta(1-\eta)^2/4, \quad \beta = 3/2, \tag{39}$$

which corresponds to $Q = 0$. We found a family of solutions for $Q > 0$ evolving from Equation 39; we first slowly increased Q and then increased Q in larger increments up to approximately $Q = 8000$. For continuation we used linear interpolation of the solutions obtained for Q_1 and Q_2 ($Q_1 < Q_2$) to provide the guess for the solution at $Q = Q_3 > Q_2$. Above $Q = 8000$, β began to change more rapidly, and we replaced (38) by

$$Q' = 0, \tag{40}$$

in order to prescribe β and compute Q and f. We continued by linear interpolation (as with Q) until $\beta = -0.75$ where $Q = 20{,}000$. A summary of the numerical results is provided in Figure 2.

For $Q \lesssim 6900$ the solutions had 2 cells; see Figure 2. Above $Q \approx 6900$, a third cell appeared and increased in strength as β was decreased; see Figure 2. A local maximum in Q was reached at $Q = 8614.48$, $\beta = -0.0675$; a local minimum in Q was reached at $Q = 8128.32$, $\beta = -0.21$. Thus for $8128.32 < Q < 8614.48$ we found three distinct solutions of the TPBVP, Equations 36 and 37. Figure 3 compares the three solutions of $Q = 8600$ with that for $Q = 500$. It is

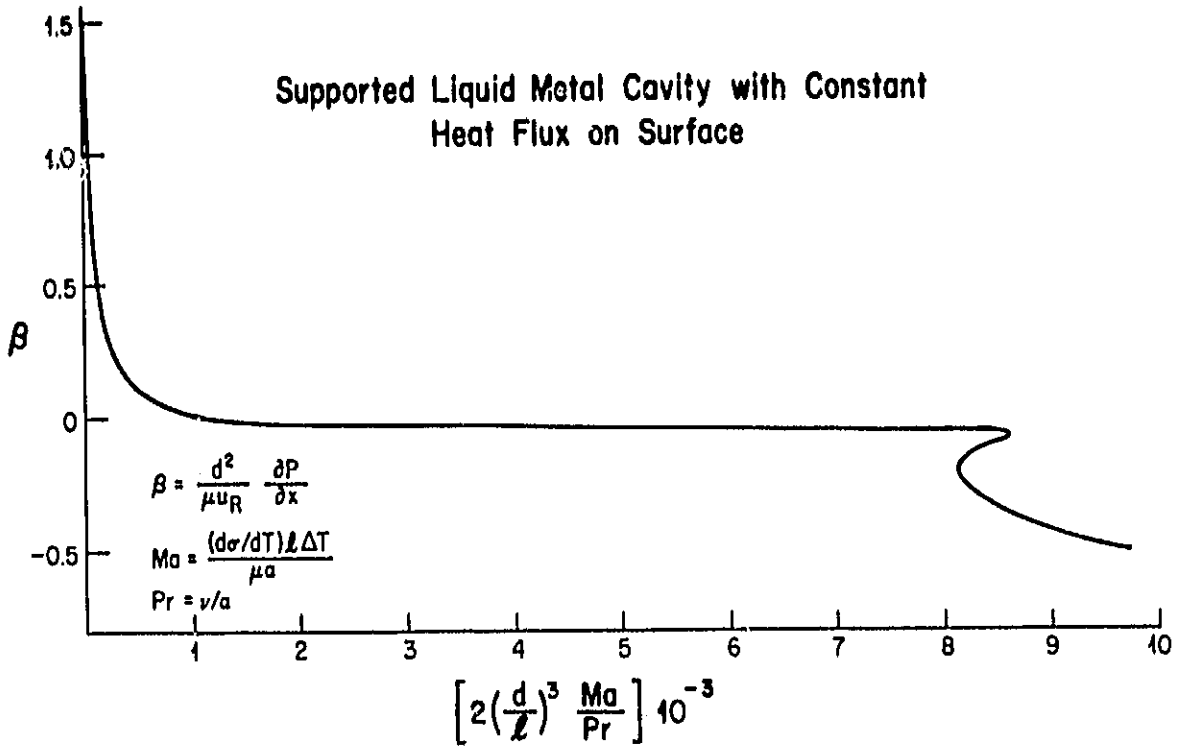

Figure 2. Results of numerical evaluation of TPBVP, Eqns. 36 and 37.

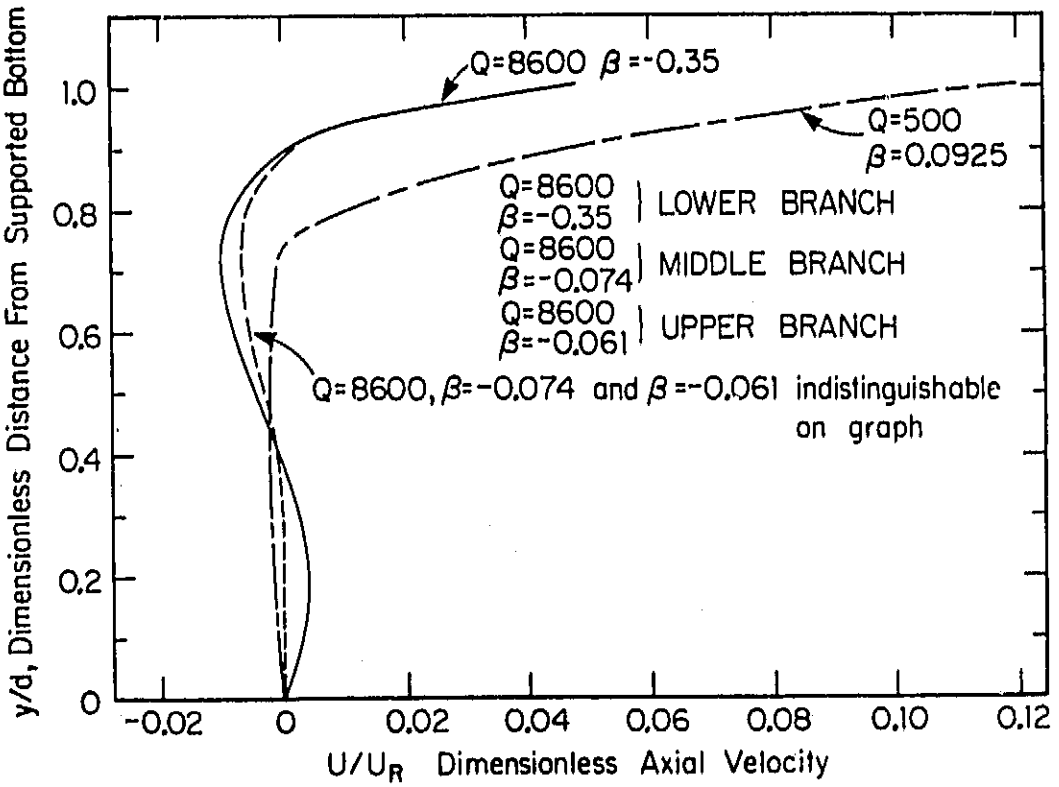

Figure 3. Numerical predictions of axial velocity versus height above the support surface.

seen that the differences between the velocity distributions on the middle and lower parts of the branch are so small as to be indistinguishable on the figure.

The rapid change in β with Q for $0 \leq Q \leq 10^3$ shows clearly that nonlinear effects are important in Equation 36 even when the Marangoni number is relatively small.

Now let us calculate the deflection of the surface and determine how it depends on the parameters of the system. To do this, substitute Equations 35a,b into 31c, together with $h = h_o + h_1\varepsilon$, and by equating coefficients of ε one obtains $h_o = 0$ and for $H_1 = h_1/d$ the equation

$$\frac{d^2H_1}{dx_1^2} = \left[4ARe\ f'(0) + \frac{p_o d^2}{\mu\nu} + \frac{\beta}{A} Re\ x_1^2\right] \tag{41}$$

with the conditions that the deflection at the ends is zero and that the liquid just fills the cavity. To avoid the complications associated with the end-effects we take $\ell = L$ for the purpose of calculating H_1. Thus

$$H_1(-\ell) = H_1(\ell) = \int_{-1}^{1} H_1\, d\, x_1 = 0. \tag{42}$$

Then the final result for h is

$$h/d = \frac{\beta}{60}\frac{Re}{A}\varepsilon(1 - 5x_1^2)(1 - x_1^2). \tag{43}$$

Equation 43 shows that the deflection is small because ε is small, that it increases with Re/A and that its sign depends on the sign of β. However, it must exist in order to make the pressure distribution given by $\frac{d^2}{\mu U_R}\frac{\partial p}{\partial x} = \beta$ consistent with the boundary condition given by Equation 31c.

Sen and Davis (20) have performed an interesting analysis of capillary flow in a slot heated from the side (a half zone) by using the matching procedure suggested by Cormack, Leal and Imburger (26) for natural convection in a slot. In this way they take end-effects into account. However, they assume that the nonlinear terms in the momentum equation can be neglected and perform an analysis for small values of d/ℓ, which they use as their perturbation parameter. Their result, to the first order, is

$$\frac{h}{d} = \frac{Re}{8A}\varepsilon[x_1 - 3x_1^2 + 2x_1^3], \tag{44}$$

where x_1 is the dimensionless distance from the hot wall in their case.

One cannot compare Equations 43 and 44 quantitatively because they apply to different configurations and therefore the distribution of h with x is different. However, it is interesting to compare these results qualitatively. Let us look at the main point

of similarity first. In the limit Re → 0, $\beta = 3/2$, and for this value of β, Equation 43 predicts a maximum deflection of 0.025 Rec/A while Equation 44 predicts 0.012 Rec/A. Obviously, the parameter, $\mathrm{Rec/A} = \frac{\left|\frac{d\sigma}{dT}\right| \Delta T}{\sigma_o (d/\ell)^2}$ on which the deflection depends is the same in both cases. We note also that this parameter is inversely proportional to $(d/\ell)^2$. Thus the smaller (d/ℓ) is, the larger the fractional deflection, h/d. On the other hand in the linear flow case Equation 43 predicts a larger deflection than Equation 44; this may be due to the neglect of end-effects in our case or the fact that heating from the side is studied by Sen and Davis and we have considered surface heating. The most important difference between Equations 43 and 44 is the appearance of β, which depends on the parameter $2(d/\ell)^3$ Re and therefore reflects the nonlinear terms in the Navier-Stokes equations. For a fixed (d/ℓ) one sees from Figure 2 that h/d first decreases with Re because β decreases rapidly, and then h/d increases with Re because β remains relatively constant up to Re ~8000.

Figure 2 shows that values of β change rapidly from positive to negative as $2\left(\frac{d}{\ell}\right)^3 \mathrm{Re}$ increases from zero to a little over 1100. Beyond a value of $2\left(\frac{d}{\ell}\right)^3 \mathrm{Re} \sim 6900$ a third cell appears, and at about 8100 multiple solutions for β appear after it has changed very slowly from about 1100 to 8000. The rapid changes in β at small values of $2\left(\frac{d}{\ell}\right)^3 \mathrm{Re}$ suggest that nonlinear effects play a decisive role in the behavior of the deflection, h/d, in Marangoni flow.

We speculate that the existence of multiple solutions to the Navier-Stokes equations for surface tension driven flow in a cavity is evidence of instability in this system, and this suggests the need for a stability analysis of the velocity profiles. It should be noted that the simplified model of the molten zone which we are using does not include the blocking effect of the solid-liquid interface at $x = \pm L$.

Calculations by Gill et al. (14), in which a similar simplified model was used for a disk shaped molten zone, agreed well with more detailed finite difference calculations, except in the immediate neighborhood of the solid liquid interface. Both types of calculations for the molten disk suggested that only one steady-state similarity solution exists and that β changes rapidly with $2\left(\frac{d}{\ell}\right)^3 \mathrm{Re}$ so that nonlinear effects also are important in that configuration.

The disk problem was reduced to equations similar to Equations 36 and 37 except, for the disk, the term ff'' is replaced by $2ff''$. Therefore, the term $v\frac{\partial u}{\partial y}$ is weighted more heavily compared $u\frac{\partial u}{\partial x}$ in the disk than in the cavity and this eliminates multiple solutions. This seems to mean that a relative increase in the convection of x-direction momentum normal to the free surface compared to its convection parallel to the free surface favors stability in the zone. However, a stability analysis is required to confirm this hypothesis.

Smith and Davis (27) have carried out an interesting stability analysis on liquid layers in a slot heated from the side. They neglected end effects and the nonlinear inertia terms in their base-flow velocity distribution and identified three types of instabilities: stationary roll cells, hydrothermal waves and surface waves. In systems with return flows, as is the case in floating or supported zones, stationary roll cells were shown not to exist in slots heated from the side. Surface waves were found to be the prevailing cause of instability at very low Pr. However, it seems tenuous to try to extrapolate their results to the return flows with significant inertial effects and surface heating which we studied because the nonlinear inertia terms have a profound influence on the velocity profile, the surface deflection and the pressure distribution; therefore they would influence strongly all modes of instability.

It is clear that vigorous thermocapillary flows with surface velocities on the order of 10 cm/sec may exist in low Prandtl number liquid metal or semiconductor zones. These flows no doubt have a profound effect on the temperature and solution distribution in these zones, and thereby they affect crystal quality. This conclusion is consistent with that drawn by Wilcox and coworkers, (28) and (29), who first called attention to the potential importance of surface tension driven flows in float zone solidification. Schwabe and Scharmann (16) have recently summarized experimental investigations on a wide variety of high Pr number fluids. Surface velocities have been directly measured in transparent fluids with Pr numbers varying from 0.3 for molten KCl to over 1000 for silicon oils and molten glass. The study on molten glass, for example, recently reported by McNeil et al. (30) with both top and bottom heating of a liquid bridge reported flows of roughly equal velocity in the range of 0.1 to 1 cm/s. This study and the several others listed by Schwabe and Scharmann (16) confirm the predominance of surface-tension flow over natural convection even at 1 g, and it seems reasonable that this same conclusion will apply to liquid metals and semiconductors at Pr numbers which fall into the .01 to .03 range.

Literature Cited

1. Pfann, W. G. Trans. Met. Soc. AIME 1952, 194, 747.
2. Shaw, J. S. "Zone Melting and Applied Techniques" in "Crystal Growth"; B. R. Parryslin, Ed., Pergamon Press, New York, 1975.
3. Smith, V. G.; Tiller, W. A.; Rutter, J. W. Can. J. Phys. 1955, 33, 723.
4. Burton, J. A.; Prim, R. C.; Slichter, W. C. J. Chem. Phys. 1953, 21, 1987.
5. Kays, W. M.; Crawford, M. E. "Convective Heat and Mass Transfer"; 2nd Ed., McGraw Hill, New York, 1980.
6. Stewartson, K.; ZAMP 1958, 9a, 276.
7. Gill, W. N.; Zeh, D. W.; del Casal, E. ZAMP 1965, 16, 539.
8. Levich, V.; "Physicochemical Hydrodynamics"; Prentice Hall, Inc.: Englewood Cliffs, N.J., 1962.
9. Acrivos, A.; A I Ch E Journal 1960, 6, 584.
10. Lighthill, M. J. Proc. Rog. Soc. 1950.
11. Gill, A. E. J. Fluid Mech. 1974, 64, 577.

12. Carruthers, J. R. J. Crystal Growth 1976, 32, 13.
13. Milson, J. A.; Pamplin, B. R. Prog. Crystal Growth Charact. 1981, 4, 195.
14. Gill, W. N.; Kazarinoff, N. D.; Hsu, C. C.; Noack, M. A.; Verhoeven, J. D. "Thermocapillary Driven Convection in Supported and Floating Zone Crystallization"; COSPAR, Advances in Space Research: Pergamon Press, 1984.
15. Preisser, F.; Schwabe, D.; Scharmann, A. J. Fluid Mech. 1983, 126, 545.
16. Schwabe, D.; Scharmann, A. "Microgravity Experiments on the Transition from Laminar to Oscillatory Thermocapillary Convection in Floating Zones"; COSPAR, Advances in Space Research: Pergamon Press, to be published in 1984.
17. Yih, C. S. Phys. Fluids 1968, 11, 477.
18. Ostrach, S. "Physicochemical Hydrodynamics"; V. C. Levich Festschrift (ed. D. B. Spalding) 1977, 2, 571.
19. Ostrach, S. Ann. Rev. Fluid Mech. 1982, 14, 313.
20. Sen, A. K.; Davis, S. H. J. Fluid Mech. 1982, 121, 163.
21. Cowley, S. J.; Davis, S. J. Fluid Mech. 1983, 135, 175.
22. Roberts, G. O. Geophys. Astrophys. Fluid Dyn. 1977, 8, 197 and 1979, 12, 235.
23. Carter, L; Gill, W. N. AIChE Journal 1964, 10, 330.
24. Brady, J; Acrivos, A. J. Fluid Mech. 1981, 112, 127 and 1982, 115, 427.
25. Deuflhard, P. "Recent Advances in Multiple Shooting Techniques" in Computational Techniques for Ordinary Differential Equations, Caldwell and Sayer, Eds, Academic Press, New York, 1980.
26. Cormack, D. E.; Leal, L. G.; Imberger, J. J. Fluid Mech. 1974, 64, 577.
27. Smith, M. K.; Davis, S. H. J. Fluid Mech. 1983, 132, 119 and 145.
28. Chang, C. E.; Wilcox, W. R. Int. J. Heat Mass Trans. 1976, 19, 335.
29. Clark, P. A.; Wilcox, W. R. J. Crys. Gr. 1980, 50, 461.
30. McNeil, T.; Cole, R.; Subramanian, S. "Surface Tension Driven Flow in Glass Melts and Model Fluids" in Materials Processing in the Reduced Gravity of Space, Guy Rindone, Ed, Elsevier, 1982, p. 289-299.

III. Summaries of experimental work carried out during the final reporting period, October 1, 1983 to June 30, 1984.

Experiment 1, Detection of Oscillatory Flow

Experimental Design

The aim of initial experiments was to detect oscillatory Marangoni flow in the tin disk floating zone geometry (DFZ) utilizing a thermocouple to detect oscillations produced by oscillatory fluid motion. Theoretical models predict values of either a surface Reynolds number or a Marangoni number at which one expects to see the onset of oscillatory flow. Therefore, an initial phase of our experiments was to utilize the computer program developed by C. C. Hsu (which utilizes finite difference techniques to model our DFZ geometry) in order to design an experiment which would allow us to achieve high values of $(Ma)_s$, the Marangoni number utilized by Schwabe, and $(Re)_R$, a surface Reynolds number utilized in our theoretical analyses.

The geometric variables of the DFZ geometery are illustrated schematically in Figure 1. Four parameters enter into the design, the total tin disk radius, R, the molten tin disk radius, ℓ, the heater radius, a, and the disk height, d. The two dimensionless parameters are related to controllable experimental parameters as follows:

$$(Ma)_s = \frac{|d\sigma/dT| \cdot \Delta T \cdot \ell}{\mu\alpha} \qquad (1)$$

where $d\sigma/dT$ = temperature derivative of surface tension, ΔT = temperature difference between hot and cold sinks, ℓ = radius of the molten zone, μ = viscosity and α = thermal diffusivity.

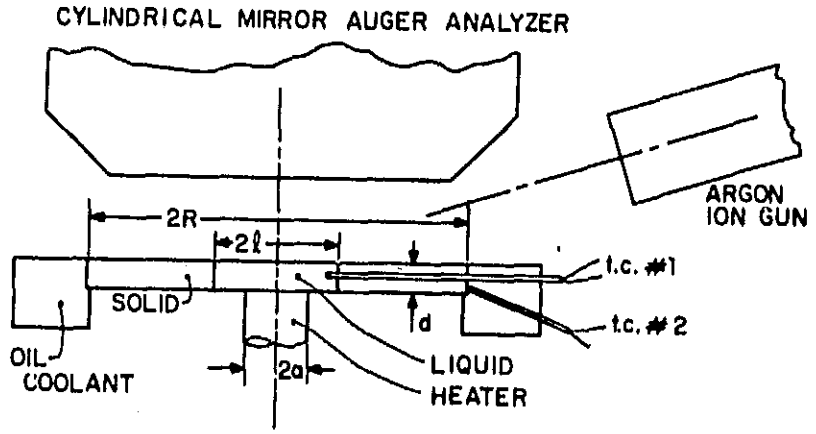

Figure 1. The disk float zone (DFZ) geometry.

$$(Re)_R = \frac{\rho U_R d}{\mu}, \tag{2}$$

where ρ = density, and U_R is a reference velocity defined as,

$$U_R = \frac{|d\sigma/dT| \cdot \Delta T_R}{\mu} \tag{3}$$

where ΔT_R is a reference temperature difference defined as

$$\Delta T_R = \frac{P}{\pi k_\ell d} \tag{4}$$

where k_ℓ = liquid thermal conductivity and P is the power into the disk, which may be evaluated from the heat flow in the solid portion of the disk,

$$P = \frac{2\pi k_s d (T_{mp} - T_c)}{Ln(R/\ell)} \qquad (5)$$

where k_s = solid thermal conductivity, T_{mp} = melting point temperature, T_c = cold sink temperature.

There are two major limitations upon our experimental system, the temperature of the cold sink cannot go below 40 to 50°C and still maintain good control and the high temperature cannot go above 500 to 550°C because of limitations involving a solder joint in the heater design, plus a solder used to attach the heating element. Our design objective is to achieve conditions which correspond to a value of $(Ma)_s$ greater than 7400 within these limitations on temperature. The value of 7400 is that value found by Schwabe[1] to cause oscillatory flow in $NaNO_3$ under cylindrical geometric conditions. Based on initial studies (Annual Report 1983) we chose for the optimum conditions within the power limitations of our present heater design the following conditions: a = 3 mm, d = 1 mm, s = 6 mm, and R = 15 mm. The computer output for these conditions gave a dimensionless temperature at the heater center, r = 0 and the heater interface, Z = 0, $[\theta(0,0)]$ as a function of $(Re)_R$ from which we obtained the temperature at the heater interface,

$$T_h = 232 + \theta(0,0) \cdot \Delta T_R \qquad (6)$$

where ΔT_R is given by Eqn. 4. The value of $(Ma)_s$ is related to $(Re)_R$ as,

$$(Ma)_s = (Re)_R \, Pr \left(\frac{\ell}{d}\right) \theta(0,1) \tag{7}$$

where $\theta(0,1)$ is the dimensionless temperature at r = 0 and the upper disk surface. By combining equations 2 to 5 one obtains an expression for $(Re)_R$ as a function of the controlled parameters of the experiment.

$$(Re)_R = \frac{2\rho d \left|d\sigma/dT\right| k_s (T_{mp} - T_c)}{\mu^2 k_\ell \ln (R/\ell)} \tag{8}$$

From Eqns. 4 through 8 and the computer output for $\theta(0,0)$ and $\theta(0,1)$, the significant parameters are given in Table I for the conditions, R = 15 mm, ℓ = 6 mm, d = 1 mm, ρ = 7 gms/cm^2, $|d\sigma/dT|$ = 0.17 dynes/cm-°C, μ = 0.018 dyne-s/cm^2, K_s = 0.305 j/cm-C, k_ℓ = 0.06 j/cm-C, a = 3.0 mm and Pr = 0.014.

Table I. Computer Model Predictions

$(Re)_R$	$(Ma)_s$	Hot Temp., T_h	Cold Temp, T_c	Power, P
10^4	482	249°C	225°C	2.65 watts
5×10^4	2200	314°C	200°C	13.2 watts
10^5	4370	388°C	167°C	26.5 watts
5×10^5	17800	882°C	- 90°C	133 watts

These values along with some others have been plotted as Figure 2. From these plots it is seen that a $(Ma)_s$ value of 7400 is achieved at

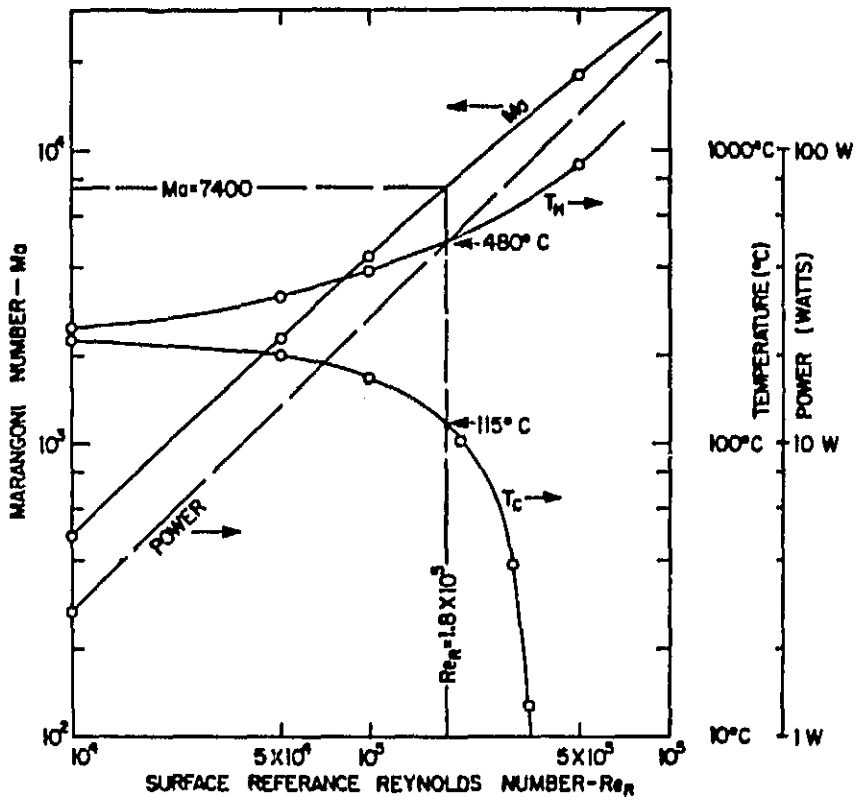

Figure 2. Plots of the data shown in Table I, for Sn with R = 15 mm, ℓ = 6 mm, d = 1 mm and a = 3 mm.

a T_h value of 480°C and a T_c value of 115°C. There are two experimental parameters which we can easily control and measure, T_c the cold sink temperature using thermocouple number 2 (t.c. #2) on Fig. 1 and ℓ, the radius of the molten Sn zone. T_c is controlled by the temperature of the hot oil bath. For a given T_c the value of ℓ is adjusted by power input to the heater and it is monitored by means of a telescope. Therefore, from the plot of Fig. 2 we may evaluate both $(Re)_R$ and $(Ma)_s$ for any given value of T_c and the power input conditions adjusted

to give $\ell = 6$ mm. To achieve high values of $(Re)_R$ and $(Ma)_s$ one needs to lower T_c. Selecting a minimum achievable T_c of 70°C gives a maximum obtainable $(Re)_R$ value for this design of 2.5×10^5 which corresponds to $(Ma)_s = 10{,}000$ which is just slightly above the most recently reported values of Schwabe[2] for his $NaNO_3$ fluid.

Experimental Results

Experiments were carried out in our UHV system. Utilizing a cold sink temperature of 166°C we were able to produce an 11.7 mm diameter zone with a clean upper surface at a value of Ma = 4300 (see section II for details). This was the maximum Ma possible with our heater design (see 1983 annual report for heater design details). There are two points in the design, a solder joint and a current limitation on a vacuum feedthrough, which set this limit. A new design has been developed which should allow Ma value of 10^4 to be achieved. As may be seen from Fig. 2 the heater must be capable of raising the molten tin temperature to 570°C at the heater interface, which means the heater itself must operate somewhere above 600°C.

Our experiments have not detected any temperature oscillations due to Marangoni convection. This could mean either (1) temperature oscillations are in fact not present, or (2) temperature oscillations are present, but they occur at frequencies too high for our measuring system to detect. Clearly, it was very important for us to evaluate the frequency response of our thermal measuring system, and experiments were carried out to this effect.

A frequency generator was set up, attached to our system and experiments were carried out under several configurations. It was

quickly determined that the best frequency response was obtained by feeding the thermocouple output directly into the chart recorder. (Initially we had utilized a Keithly 181 nanovoltmeter and although the output of this device allowed improved sensitivity it greatly reduced frequency response). Measurements were made on the chart recorder using the same sensitivity scale as used for recording temperature in the experiments. Sine wave voltages of amplitudes varying from 10 to 40 μV were measured as a function of frequency from 0.02 to 20 Hz. The attenuation of the amplitude was determined and the results are presented as the reciprocal of the fractional attenuation of amplitude versus frequency on curve A of Fig. 3.

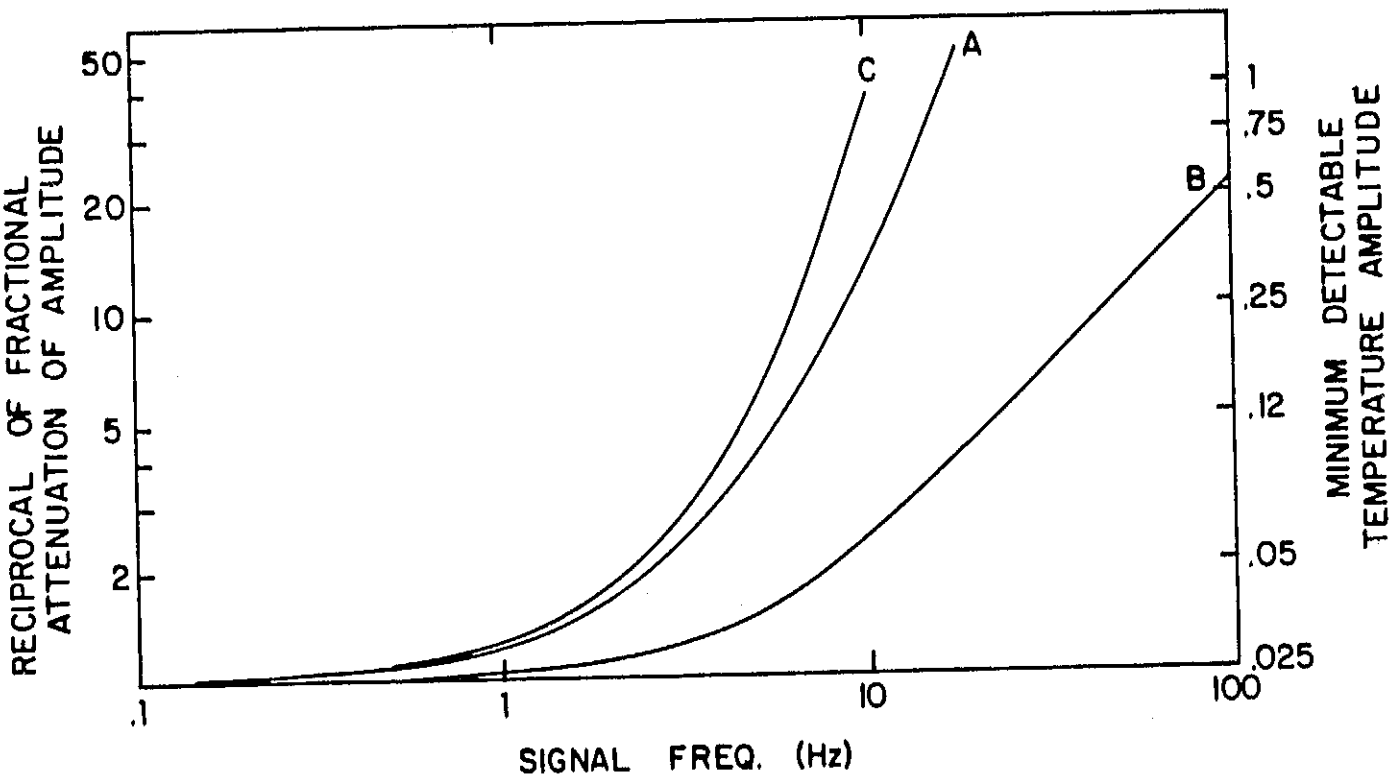

Figure 3. Response of thermocouple output as a function of signal frequency.

In general our experimental work shows that we can detect a minimum amplitude of oscillations on the order of 1 μV with our type K thermocouples. The minimum detectable temperature amplitude given as the right hand scale of Fig. 3 is for this 1 μV detection limit on the amplitude of the oscillation. Referring to curve A, Fig. 3, this means that at 10 Hz in order to detect a signal oscillation its amplitude would have to be > 13.5 μV, which corresponds to an oscillating temperature amplitude of 0.34°C with our type K thermocouples, as is shown on the right hand ordinate of the plot of Fig. 3.

This approach assumes that the thermocouple itself has an infinitely fast time response and we are limited only by the response of our recorder system. Experiments on the time response of small thermocouples in molten metal environments are available in the literature[3] and they show that a 10 mil (250 μm) thermocouple has a time constant, τ, of 35 ms in molten Sn-Pb.

This finite time response will also reduce the amplitude of an oscillating signal and it may be shown that the reciprocal of the fractional attenuation of the amplitude of the signal is given as $[1 + (\omega\tau)^2]^{1/2}$, where ω is frequency in radians per second. This function is shown as curve B on Fig. 3. The total attenuation of the signal is then given by curve C which is the product of A and B.

These results predict the following picture. With a 10 mil thermocouple having a 35 mS time constant attached to our chart recorder system we should be able to detect temperature oscillations greater than or equal to the values given by the right hand ordinate using curve C. The frequency dependence of these results are summarized in Table II. From these results it is clear that temperature

Table II. Tabulation of results of Figure 1, curve C.

Frequency	Minimum Detectable Temperature Oscillation Amplitude
< 0.1 Hz	.025°C
1 Hz	.031°C
2 Hz	.045°C
5 Hz	.155°C
10 Hz	.950°C

oscillations above 5 to 10 Hz are unlikely to be detected by our present system unless their temperature amplitude is quite large. The results also show that to improve the frequency of our system we can (1) reduce the diameter of the thermocouple in order to reduce its time constant, (2) increase the Seebeck coefficient of the thermocouple, and (3) improve the frequency response of our recorder system. This latter improvement could be achieved by going to a digital data acquisition system.

These results have been presented briefly in our COSPAR paper, see pages 15-16. We conclude that at Ma = 4300 in the disk system no temperature oscillations occur of frequencies less than 5 to 10 Hz.

Experiment 2, Interface Shape Evaluation

The purpose of this experiment was to detect Marangoni flow in this opaque metallic system by observing its effect upon the shape of the solid-liquid interface. The procedure would involve a set of comparison experiments. In the reference experiment the top molten Sn surface would be cleaned of oxide film with argon ion sputtering, and the shape of the solid-liquid interface formed at the point of furthest melt-out would be determined. The predicted Ma surface flow velocity toward the solid is around 25 cm/s for the Ma = 4300 experiment. Since the bottom surface of the disk has a thick oxide layer upon it we expect no Ma flow there. Hence, the rapid Ma flow on the top surface should cause the S/ℓ interface to be melted outward toward the cold sink successively further as one goes from bottom to top of the disk. Therefore in the subsequent comparison experiments one selectively oxidizes the upper surface to different oxide layer thicknesses and evaluates if some minimum oxide layer thickness is adequate to maintain the S/ℓ interface a constant distant from the cold sink from top to bottom of the disk.

The technique for marking the S/ℓ interface was simply to use a eutectic alloy, Sn-Au. This alloy was chosen because (1) Au is a noble metal and might not change the oxidation characteristics of molten Sn significantly, and (2) a eutectic occurs at only 10 wt.% Au and it has a large volume fraction of second phase, ~ 30%, while only lowering the melting point of Sn by 15°C. The microstructure of a eutectic is very sensitive to solidification conditions. Therefore, by starting with a disk of a given microstructure and melting out to radius R, one expects

to be able to easily detect the melt-out interface shape by doing metallographic analysis on sectioned disks.

Techniques were developed to prepare disks of Sn - 10 w/o Au alloys and two experiments were run with essentially identical results. It was found that after melting out the zone to a given diameter upon holding for 10 minutes or so a ridge of solid material began to be deposited all along the edge of the solid-liquid interface. In a few hours time the ridge became quite large as is shown in the sequence of photos presented in Fig. 4. Sectioning of the sample revealed that the S/ℓ interface was clearly delineated, but the presence of the ridge of solid material was too disruptive to allow meaningful interpretation of these experiments. If we could have solidified the samples before enough time passed to build up the ridge material then the experiments would have been pursued. Unfortunately, we could not clean the molten surface by sputter cleaning in less than an hour or so. This suggests cleaning the surface prior to melting. We found that it was necessary to clean the surface after additional solid was melted because oxygen and sulfur were detected at the newly melted surface, due apparently to liberated atoms from the melting. Hence, the surface could not be cleaned prior to melting and thereby be assured of no oxidation. Consequently these experiments were abandoned. The cause of the ridge buildup will not be addressed in this report. It does not occur with pure tin.

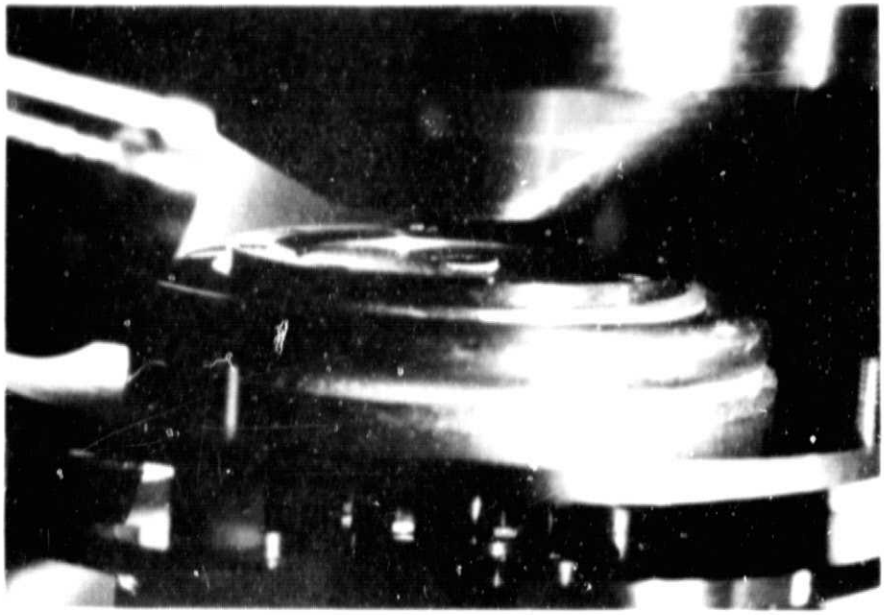

Figure 4. Photos of Sn-Au Eutectic Experiment.

(a) Photo through viewport of UHV system.

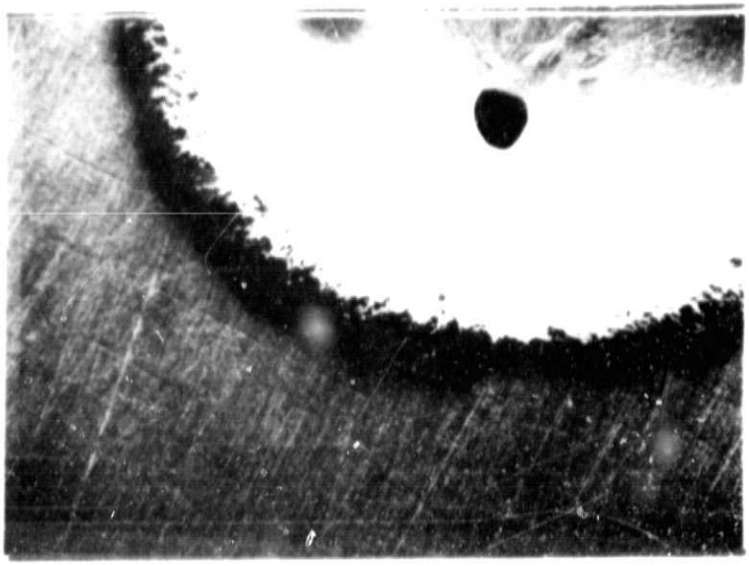

(b) SEM photo of solidified sample at 17x.

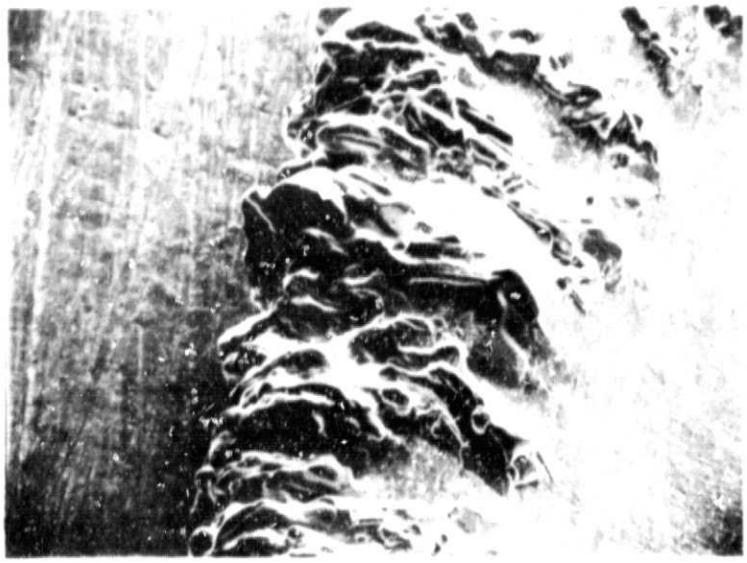

(c) SEM photo of rim area at 85x.

Experiment 3, Macrosegregation Study

The purpose of this experiment was to detect Marangoni flow in the DFZ apparatus by evaluating its effect upon macrosegregation. As with experiment 2 this technique involves a comparison study between a disk solidified with no oxide and one solidified with oxide deliberately controlled to a desired thickness level. The control experiment is the oxide free experiment where one expects very large convection velocities along the top surface, V ≅ 25 cm/s with Ma = 4300. In this case one expects an effective distribution coefficient k_e nearly equal to the equilibrium coefficient k_o. By repeating the experiment with an oxide film of sufficient strength to suppress Marangoni convection one expects the value of k_e to rise to 1 after an initial transient whose length will depend upon the rate of solidification. Hence, by measuring k_e one can indirectly evaluate the effect of convection and hence the effectiveness of oxide films upon suppression of this convection. In these experiments it was planned to measure k_e by utilizing the radioisotope Bi^{207} at levels of around 200 ppm to determine composition variations as a function of fraction solidified.

We had difficulty procuring some Bi^{207} but a source was located and an experimental technique was developed to plate out the Bi^{207} and to dope it into Sn disks at around the 200 ppm level. This work relied in part on our previous studies[5,6] with this Sn-Bi^{207} system. In addition, it was necessary to be able to control the power input to the heater in a programed way in order to solidify the disk at a constant rate. We were able to borrow a programable power supply for this work and a relatively inexpensive Apple IIe computer was purchased for the

programming. This work, coupled with the fact that our Auger CMA had to be returned to the manufacturer for maintenance (2 month turnaround) was a sufficient delay that the first Bi^{207} experiment was not run prior to our June 30 termination date.

References

1. F. Preisser, D. Schwabe, and A. Scharmann, J. Fluid Mech. 126, 545 (1983).

2. D. Schwabe and A. Scharmann, Paper G.1.2.4 COSPAR Conference, Graz, Austria, July 1984.

3. J. Nanigan, Namac Temperature Handbook p. L27, Namac Corp., Framingham, MA (1981/82).

4. R. P. Benedict, Fundamentals of Temperature, Pressure and Flow Measurement, p. 270, John Wiley, NY (1977).

5. J. D. Verhoeven, E. D. Gibson, and R. I. Griffith, Met. Trans. 6B, 475 (1975).

6. J. D. Verhoeven, E. D. Gibson and B. Beardsley, Met. Trans. 6B, 349 (1975).

☆U.S. GOVERNMENT PRINTING OFFICE 1985—544-048/10083